Sm^{3+} IONS DOPED BOROSILICATE GLASS FOR VISIBLE PHOTONIC DEVICE APPLICATIONS

A PROJECT REPORT

SUBMITTED IN COMPLETE FULFILLMENT OF THE REQUIREMENTS

FOR THE AWARD OF THE DEGREE

OF

MASTER OF SCIENCE

IN

APPLIED PHYSICS

Submitted by:

ASHISH MAKHLOGA (2K19/MSCPHY/33)

VIDESH KUMAR (2K19/MSCPHY/02)

Under the supervision of

PROF. A. S. RAO

APPLIED PHYSICS

DELHI TECHNOLOGICAL UNIVERSITY

Bawana Road, Delhi-110042

MAY 2021

DECLARATION

APPLIED PHYSICS

We/I hereby certify that the work which is presented in the Major Project-II/Research Work entitled in fulfilment of the requirement for the award of the **Master of Science in Physics** and submitted to the **Department of Applied Physics, Delhi Technological University,** Delhi is an authentic record of my/our own, carried out during a period from August 2020 to May 2021, under the supervision of **Prof. A.S. Rao**.

The matter presented in this report/thesis has not been submitted by us/me for award of any other degree of this or any other Institute/University. The work has been published/accepted/communicated in SCI/SCI expanded/SSCI/Scopus indexed journal OR peer reviewed Scopus indexed conference with the following details.

Title of the Paper: "Sm^{3+} ions doped borosilicate glass for visible photonic device applications"
Author names (in sequence as per research paper): Ashish Makhloga, Videsh Kumar, and A.S. Rao
Name of Conference/Journal: 6th International Conference on Advanced Production and Industrial Engineering (ICAPIE) – 2021
Conference Dates with venue (If application): June 18-19, 2021
Have you registered for the reference (Yes/No)? : Yes
Status of paper (Accepted/Published/Communicated): Accepted
Date of paper communication: 10 May 2021
Date of paper acceptance: 13 May 2021
Date of paper publication: October 2021

Name (Roll no): Ashish Makhloga (2K19/MSCPHY/33), Videsh Kumar (2K19/MSCPHY/02)

SUPERVISOR CERTIFICATE

To the best of my knowledge, the above work has not been submitted in part of full for my Degree to this University or elsewhere. I further certify that the publication and indexing information given by the students is correct.

Place: New Delhi
Date: 31 May 2021

(SUPERVISOR SIGN)
Prof. A.S. Rao.

NOTE: PLEASE ENCLOSE RESEARCH PAPER ACCEPTANCE/PUBLICATION/COMMUNICATION PROOF ALONG WITH SCOPUS INDEXING PROOF (https://icapie.com).

ACCEPTANCE CERTIFICATE

Springer

ICAPIE DTU

TRANSACTIONS

tribologyinindustry

Certificate

Dear Author(s): Ashish Makhloga, Videsh Kumar and Allam Srinivasa Rao

Paper ID: 473

Paper Title: Sm3+ ions doped Borosilicate glasses for visible photonic device applications

This is to enlighten you that the above manuscript has been appraised by the editors of LNME and is accepted for the **6th International Conference on Advanced Production and Industrial Engineering (ICAPIE)- 2021 to be held during June 18-19, 2021**. The paper is recommended for publication in **Lecture Notes in Mechanical Engineering (Scopus Indexed publication of Springer Nature), ISSN: 2195-4356**. The manuscript has been submitted to Springer in May 2021 and will be online during October 2021.

Finally, the team of CAPIER DTU and ICAPIE-2021 would like to extend congratulations to you.

Prof. Ranganath M Singari
(Conference Chair, ICAPIE-2021)

Dr. Harish Kumar
(Convener, ICAPIE-2021)

REGISTRATION RECORD

5/11/2021 ICAPIE 2021

TECHNOSCIENCE

ICAPIE 2021

Program name

6th International Conference on Advanced Production and Industrial Engineering

Program Description

June 18-19, 2021

Fee breakup(Round 3)

Students(UG/PG/Ph.D) : 7500
Faculty : 9000
Delegates from Industry/R& D Centers : 9500
Fee beyond 10 pages : 500/page

Name of the organiser

Centre for Advanced Production and Industrial Engineering Research (CAPIER) ,Delhi Technological University, Delhi

Contact Us:

icapie.dtu@gmail.com

icapie.dtu@gmail.com

₹ 8000.00
Payment Successful!

Thank you for registration in ICAPIE-2021

Share Your Experience

Payment ID: pay_H9VgT8zYvd8dco
A confirmation email has been sent to you

Razorpay

Want to create payment pages for your business? Visit Razorpay Payment Pages and get started!

Please report this page if you find it to be suspicious
Report Page

https://pages.razorpay.com/ICAPIE3 1/1

PLAGIARISM REPORT

turnitin

Report 01 without t and f.pdf
May 30, 2021
6762 words / 34931 characters

Report 01.pdf

Sources Overview

9%
OVERALL SIMILARITY

No.	Source	Type	Similarity
1	www.fulviofrisone.com	INTERNET	<1%
2	propertibazar.com	INTERNET	<1%
3	Jnos Schanda. "CIE Colorimetry", Colorimetry, 07/07/2007	CROSSREF	<1%
4	link.springer.com	INTERNET	<1%
5	www.freepatentsonline.com	INTERNET	<1%
6	N. Premjit Singh, N. Premananda Singh, N. Rajmuhon Singh, N. Mohondas Singh. "Photoluminescence studies of CdWO4:Sm3+ phosp...	CROSSREF	<1%
7	Ho Chi Minh University of Technology and Education on 2020-09-18	SUBMITTED WORKS	<1%
8	P. Rekha Rani, M. Venkateswarlu, Sk. Mahamuda, K. Swapna, Nisha Deopa, A.S. Rao, G. Vijaya Prakash. "Structural, absorption and ph...	CROSSREF	<1%
9	West Thames College London on 2015-11-17	SUBMITTED WORKS	<1%
10	pubs.rsc.org	INTERNET	<1%
11	Adon Jose, Krishnapriya T, Twinkle Anna Jose, Saritha A C, Cyriac Joseph, P. R. Biju. " Energy transfer analysis and realization of cool t...	CROSSREF	<1%
12	Nisha Deopa, Babloo Kumar, Mukesh K. Sahu, P. Rekha Rani, A.S. Rao. "Effect of Sm3+ ions concentration on borosilicate glasses for r...	CROSSREF	<1%
13	P. Rekha Rani, M. Venkateswarlu, Sk Mahamuda, K. Swapna, Nisha Deopa, A.S. Rao. "Spectroscopic studies of Dy3+ ions doped bariu...	CROSSREF	<1%
14	University of Wales Swansea on 2021-05-13	SUBMITTED WORKS	<1%
15	eprints.uwe.ac.uk	INTERNET	<1%
16	hdl.handle.net	INTERNET	<1%
17	www.cs.bgu.ac.il	INTERNET	<1%

18	Nisha Deopa, Surandeep Kaur, Aman Prasad, Bipin Joshi, A.S. Rao. "Spectral studies of Eu3+ doped lithium lead alumino borate glas... CROSSREF	<1%
19	download.atlantis-press.com INTERNET	<1%
20	essay.utwente.nl INTERNET	<1%
21	www.coursehero.com INTERNET	<1%
22	Monash University on 2018-08-28 SUBMITTED WORKS	<1%
23	P.K. Yang, C.H. Chen. "Calibration of a sequentially reflective colorimeter using a tri-color LED", Journal of Modern Optics, 2008 CROSSREF	<1%
24	Mohit Kumar, A.S. Rao. "Concentration-dependent reddish-orange photoluminescence studies of Sm3+ ions in borosilicate glasses", O... CROSSREF	<1%
25	Mukesh K. Sahu, M. Jayasimhadri, Kaushal Jha, B. Sivaiah, A.S. Rao, D. Haranath. "Synthesis and enhancement of photoluminescent p... CROSSREF	<1%
26	P. Sailaja, Sk. Mahamuda, K. Swapna, M. Venkateswarlu, A.S. Rao. "Optical properties of Sm3+ions doped 10SrO-(10−x)Al2O3-10BaCl... CROSSREF	<1%
27	Pawar, P.P., S.R. Munishwar, and R.S. Gedam. "Intense white light luminescent Dy3+ doped lithium borate glasses for W-LED: A correla... CROSSREF	<1%
28	pt.scribd.com INTERNET	<1%
29	Delhi Technological University on 2019-01-31 SUBMITTED WORKS	<1%
30	H.A. Othman, H.S. Elkholy, I.Z. Hager. "Structural and optical investigation of undoped and Sm 3+ doped lead oxyfluoroborate glasses"... CROSSREF	<1%
31	Inter-University Accelerator Centre on 2013-11-13 SUBMITTED WORKS	<1%
32	Jawaharlal Nehru Technological University Anantapur on 2013-08-19 SUBMITTED WORKS	<1%
33	Monash University on 2018-10-20 SUBMITTED WORKS	<1%
34	Nisha Deopa, A.S. Rao, Ankur Choudhary, Shubham Saini, Abhishek Navhal, M. Jayasimhadri, D. Haranath, G. Vijaya Prakash. "Photolu... CROSSREF	<1%
35	P.P. Pawar, S.R. Munishwar, D.D. Ramteke, R.S. Gedam. "Physical, structural, thermal and spectroscopic investigation of Sm2O3 doped... CROSSREF	<1%
36	University of Strathclyde on 2016-04-01 SUBMITTED WORKS	<1%
37	www.hindawi.com INTERNET	<1%
38	V. Murali Krishna, Sk. Mahamuda, P. Rekha Rani, K. Swapna, M. Venkateswarlu, A.S. Rao. "Effect of samarium ions concentration on p... CROSSREF	<1%

Excluded search repositories:

- None

Excluded from Similarity Report:

- Bibliography

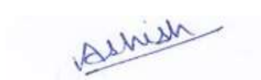

Excluded sources:

- None

DELHI TECHNOLOGICAL UNIVERSITY

(FORMERLY Delhi College of Engineering)

Bawana Road, Delhi-110042

ACKNOWLEDGEMENT

In performing our major project, we had to take the help and guideline of some respected persons, who deserve our greatest gratitude. The completion of this assignment gives us much pleasure. We would like to show our gratitude **Prof. A. S. Rao**, mentor for major project. Giving us a good guideline for report throughout numerous consultations. We would also like to extend our deepest gratitude to all those who have directly and indirectly guided us in writing this assignment.

Many people, especially **Dr. Arti Yadav (PDF)**, our classmates and team members itself, have made valuable comment suggestions on this proposal which gave us an inspiration to improve our assignment. We thank all the people for their help directly and indirectly to complete our assignment. In addition, we would like to thank Department of Applied Physics, Delhi Technological University for giving us the opportunity to work on this topic.

Ashish Makhloga

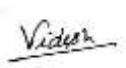

Videsh Kumar

DELHI TECHNOLOGICAL UNIVERSITY

(FORMERLY Delhi College of Engineering)

Bawana Road, Delhi-110042.

ABSTRACT

An intense reddish-orange colour radiating Samarium doped Aluminium Calcium borosilicate (BSACS) glasses were synthesized with the help of the melt-quench method to analyze the photoluminescence properties using characterization methods like XRD, FT-IR, photoluminescence (PL) excitation, PL emission, and PL decay. XRD and FT-IR reveal the non-crystalline behavior along with the presence of numerous functional groups in BSACS host glass correspondingly. Under 402 nm excitation, three major peaks were found in the emission spectra which perfectly resembles to $^4G_{5/2} \rightarrow {}^6H_{5/2}$ (562 nm), $^4G_{5/2} \rightarrow {}^6H_{7/2}$ (599 nm), and $^4G_{5/2} \rightarrow {}^6H_{9/2}$ (646 nm) transitions of Samarium ions. $^4G_{5/2} \rightarrow {}^6H_{9/2}$ transition at 599 nm is comparatively more intense and noticeable. PL decay observed for $^4G_{5/2}$ state reveals the exponential nature in which curves are fitted by using bi-exponential and tri- exponential fitting to assess the practically measured lifetimes (τ_{exp}). It is observed that the τ_{exp} values are decreasing with increasing Samarium ion concentration due to the cross-relaxation energy transference. All of the findings indicate that Sm^{3+} doped borosilicate glass is suitable for its usage in visible reddish orange photonic devices.

CONTENTS

LIST OF TABLES

LIST OF FIGURES

LIST OF SYMBOLS, ABBREVIATIONS

LED - Light emitting diode

RE - Rare Earth (Metals)

CCT - Correlated Colour Temperature

FWHM - Full Width at Half Maximum

CIE - Commission International De L' Eclairage

UV - Ultraviolet

PL -Photoluminescence

PLE -Photoluminescence Excitation

XRD - X-ray Diffraction

CVD - Chemical Vapour Deposition

CMF- Colour matching functions

τ_{avg} - Average life time

λ - wavelength of X-ray,

θ - incident angle of X-ray,

n - order of reflection (an integer),

d - spacing between diffracting plans.

T - Temperature

c - Speed of light

h - Planck's constant

K_B - Boltzmann's constant.

$\bar{x}(\lambda)$, $\bar{y}(\lambda)$, $\bar{z}(\lambda)$ - Colour matching functions

(x, y) - Colour coordinates

CHAPTER 1

INTRODUCTION

1.1 Borosilicate Glass

Modern technology linked to optical devices have seen the usage of rare earth (RE) ions doped oxide glasses. Because of their large number of applications, these are much important for the advancement of different types of optoelectronic devices like display screens, waveguides, solid-state laser, reflecting windows and sensors, etc. The materials which show glass transformation behaviour are known as glass. Borosilicate glass is a specialized type of glass which is prepared by adding Boron to the glass production process. It was first developed by Otto Schott in late 19^{th} century in Jena. It was then known as Jena Glass. The word Borosilicate glass refers to a glass family that includes members that are designed for entirely different uses. Later on W.C. Taylor and Eugene Sullivan at Corning Glass further carried out the work of Otto Schott and further extended the temperature resistant properties of borosilicate glass.

What makes Borosilicate glass so special? When Boric acid was added in the fabrication of glass, the results came out were truly remarkable. Boron trioxide (B_2O_3) plays a significant role in the glass formation attributable to its high thermally stable, high transparency, low freezing point, and high RE ions solubility [1], [2]. On the other hand, Boron trioxide in glasses alone possesses high phonon energy ($1300cm^{-1}$) because of the stretching vibrations of network-forming oxides [3]. Non-radiating transitions are mainly enhanced in the presence of high phonon energies, which significantly reduce the RE ion emissions.

1.2 Batch Materials

Glass can be made by various methods, the technique that is widely accepted and used for preparation of glass is melt-quench method. In this method glasses are synthesized by melting the batch materials at optimum temperature. The method involves a selection of batch components, calculations of relative proportion of all the materials which will be used in the process, & mixing of all the compounds to give them a homogeneous mixture. In initial heating process, these compounds go through in a sequence of physical and chemical change to form melt.

Despite of the source of the components used to manufacture a particular glass, the batch materials can be classified into five categories according to their role in the process. (a) glass

former, (b)flux, (c)property modifier, (d)colorant, (e)fining agent. Classification of categories is truly based upon the purpose for which a compound is used in the process. For example, alumina is considered as a property modifier in most of the silicate glasses but it works as a glass former in aluminate glasses.

The glass former always plays a vital role in the formation of glass. There are always one or more components which works as a primary source of structure. These components as also called as network formers, or glass forming oxides in many oxide glasses. The identity of these compounds is often the source of generic name used for the glass. Authors have used SiO_2 and H_3BO_3 as glass forming oxides. Al_2O_3 also works as glass former under certain conditions. After obtaining the desired melts, it should be quenched very rapidly because Al_2O_3 alone does not form glass until these conditions are met.

Fluxes are used to get the desired melt at the lower temperature or within practical limits (<1600 ℃). Generally, we use heavy metal oxides as fluxes. They should be added in a appropriate amount so that the properties of final glass don't degrade. As the name suggests, property modifiers modify the properties of final glass and they are less effective in decreasing the melting temperature as compared to the fluxes and their addition doesn't lead to excessively high processing temperature.

The colorants are mainly used to regulate colour in glass. In almost all the cases colorants are the oxides of 3d and 4f RE (metals). Wherever we want to regulate the colour of glass, we use colorants, and they are always present in small amount as compared to the other components present in the glass.

Fining agents are added at last to remove the bubbles from the melt. They are also present in small quantities, so that they only effects minor properties of the glass.

1.3 Host matrix and activator ion

An oxide of heavy metal such as Al_2O_3 cannot act as a conventional glass former because of its small field strength and high polarizability. However, it may be built a network pyramid within the presence of oxides like B_2O_3 and SiO_2 [4]–[6]. The alkaline earth oxides for example barium, calcium, strontium, and magnesium can change the energy state so photosensitive properties of the host glass also can be changed.

Sm^{3+} ions have been widely studied spectroscopically to characterize them for optoelectronic devices and other applications [7]–[9]. Sm^{3+} doped glasses have gained much more attention because of emissions in orange and red regions showed by them due to its transition from $^4G_{5/2} \rightarrow {}^6H_J$ which is used in optical storage of high density, sensors, underwater communication, varied fluorescent tools, and colour display. Samarium shows temperature sensitivity in the related intensity of particular lines in its emission spectrum. Sm^{3+} ion radiates the energy in the visible region from higher energy excited state to lower energy states via emission with the high quantum efficiency [10]. Sm^{3+} ions are a fascinating case for studying the energy transfer process [11]. The visible fluorescence of the Sm^{3+} ion with the $4f^5$ configuration is strong reddish-orange, and is useful in applications such as optical storage devices, underwater communication, laser devices, and colour displays [12].

Recently, Nisha Deopa et al. have studied the structural and luminous nature of Sm^{3+} doped borosilicate glass and confirm the emission of the reddish-orange color under the excitation wavelength 403 nm [6]. These kinds of glasses can be used in photonic device applications [6]. In this research article, the effects of Sm^{3+} doped ions at different concentrations on the photosensitive properties of borosilicate glasses are stated. Further, RE ions doped borosilicate glasses were investigated and we have presented the optical, structural properties, and energy transfer characteristics.

1.4 Instrumentation

1.4.1 XRD Diffraction

In the electromagnetic spectrum, the wavelength range of X-rays lies between 0.01 to 10 nm. These were discovered by Wilhem Conrad Rontgens in 1895. After their discovery, these are continuously being used in the field of Science and Technology. Laue in 1912, discovered the phenomenon of X-rays diffraction from crystals. Its growth has helped in the improvements in solid-state science and chemistry. X-ray powder diffraction (XRPD) plays an important part in mineral analysis and development because several elements are not easily accessible in only one crystal. XRD is used for characterizing the crystallinity of the materials which makes it an important tool. It provides many structural properties such as averaging of measuring grain, crystallinity, and defects in the crystal. X-ray Bruker D8 Advance Diffractometer is an instrument shown in fig. 1.1. We use this instrument to record the Xrd profile.

Fig. 1.1: X-ray Bruker D8 Advance Diffractometer.

1.4.1.1 Bragg's Law

The x-ray photons are scattered by atoms in a lattice that has a periodic nature is known as XRD. The constructive interference of a monochromatic beam of X-beams dispersed at particular points from all places of cross-section planes and this constructive interference is based on Bragg's low

$$n\lambda = 2\ d\ sin\theta$$

where,

λ = wavelength of X-ray,

θ = incident angle of X-ray,

n = order of reflection (an integer),

d = spacing between diffracting plans.

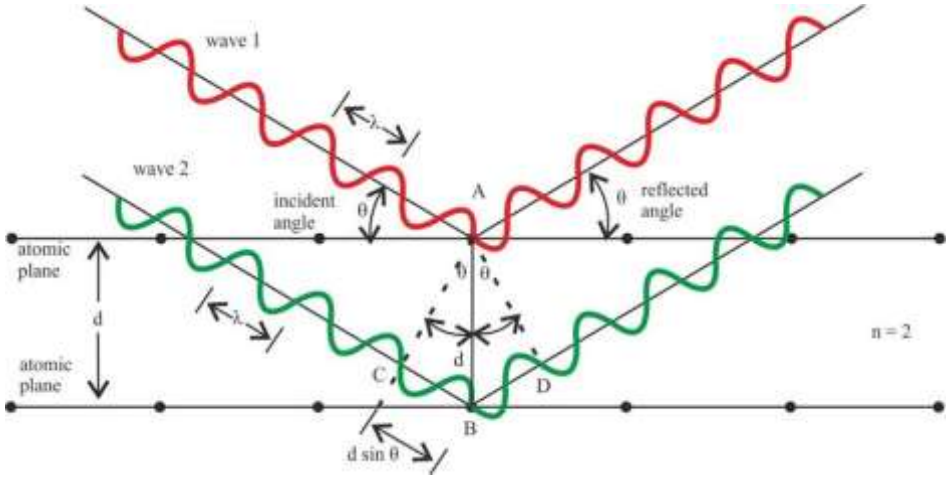

Fig. 1.2: Bragg's Law

Bragg's law can be explained by fig. 1.2. An unknown material is recognized by the intensities of various bands found out by the diffractometer which finds the powder diffraction pattern and also the *d*-values found from it contribute to this. Then this information is matched to the conventional patterns of the line which is accessible for different composites in the database of Powder Diffraction File (PDF).

1.5 SPECTROSCOPIC STUDIES

Photoluminescence is the radiation of light from a matter following the intake of light. It is made from Latin originated word luminescence and the Greek affix, photo indicating light. Photoluminescence is the luminescence caused by the consumption of photons. It is a method where a particle consumes a photon in the visible range, exciting the electron to a higher excited energy state, and then transmits a photon to a lower energy state like an electron [17].

Photoluminescence is the experimental technique used to the characterization of semiconductor nanostructures and the study of their electronic characteristics. It is induced by the illumination of the medium when energy of photons is greater than bandgap energy. Wavelengths should be almost the bandgap wavelength for photoluminescence to occur. For device characterization the necessary data can be obtained from the PL spectrum, device temperature and also intensity which depends on the irradiation intensity.

There are many advantages of PL- its capability to produce information in large quantities fast and easily; its capacity to obliquely estimate the non-radiative recombination time; its capacity to produce data about the system of energy levels and sensitivity. It is a non-destructive

technique, used on a crystal or on processed materials, needs only a little quantity of material, and complements measurements.

1.5.1 Fluorescence and Phosphorescence

Fluorescence is photoluminescence that happens much quickly following photoexcitation of a material, whereas phosphorescence is persistence photoluminescence that continued after the excitation has terminated. In other words, fluorescence is characterized as photoluminescence where there is no need for a change in a spin multiplicity in radiative transition, and phosphorescence is photoluminescence where there is a requirement of a change in a spin multiplicity in radiative transition.

Steady molecules contain sets of electrons, and molecules with single electrons are notably responsive and volatile. Electrons own a rotational momentum called 'spin' and the relevant symmetry of spins of electrons decides the belonging of electron in one of two states. If the orientation of two spins is antisymmetric then the total spin will be of zero (S = 0) while if the orientation is symmetric then the total spin will be of one (S = 1). The combination of electron spin pair which is antisymmetric S = 0 is called singlet and the three successions of spin combination states which are symmetric S = 1 states is called a triplet.

One electron from the pair is raised to an energy level which is higher when the atom absorbs a photon, and it is now said to be in an excited state. An atom's ground state is a singlet state (S_0) and because of angular momentum conservation, the photo-excited state needs to be a singlet (S_1). The decay of S_1 to S_0 is an approved shift (due to same spin multiplicity) ending in fluorescence that happens in nanoseconds time scale.

The practical applications of fluorescence include mineralogy, gemmology, drug, sensors, fluorescent labelling, stains, organic indicators, and cosmic-ray's disclosure. Fluorescent lamps and LEDs are the everyday application, where the short wavelength UV (blue) light is converted into longer wavelength (yellow) light by fluorescent coating. The fluoresce and phosphorescence can be easily understood by fig. 1.3.

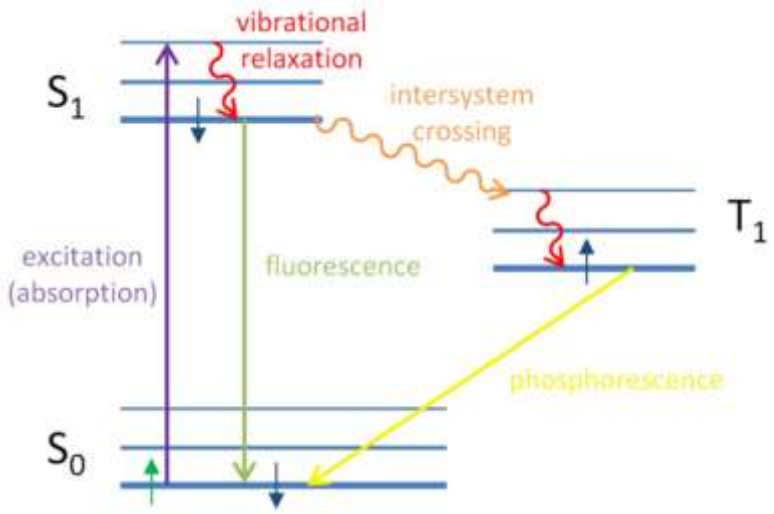

Fig. 1.3 Jablonski diagram of fluorescence and phosphorescence processes.

The molecule can also experience transition to triplet state (T_1) called intersystem crossing (ISC). ISC happens where there is a great range of spin-orbit coupling in molecules that provides translation between the S_1 and T_1 states. Metals like europium and iridium have high spin-orbit coupling strength because of the high particle and phosphorescent molecules mass. As the states own distinct spin multiplicities the decay of T_1 to S_0 is a prohibited shift, due to the angular momentum conservation. But, spin-orbit coupling eases this limitation furthermore the passage from T_1 to S_1 grows feasible. Because it is 'prohibited' the transition from T_1 to S_0 befalls on a slow-paced timescale (μs), known as phosphorescence.

1.6 Colorimetry

Thomas Young, Helmholtz, and Maxwell were firstly showing interest in colour science and they tried to understand human colour vision in the early nineteenth century. They understood how the colours can be mixed additively or subtractive which helped them putting up this theory.

Colorimetry is the science of the quantitative measurement of colour.[13] The colour measurement is done by measure the intensity of electromagnetic radiation and wavelength in the visible region. The main uses are to identify and characterize the elements that absorb light at different concentrations. It works on Beer–Lambert's law, where the proportionality between the absorbance and the concentration of a solute is shown.

In 1931, The Commission Internationale de l'Eclairage (CIE) introduced an efficient system that gives a proper determination of colour stimuli which has been used for the last 80 years and created a base for further research in it.

The electromagnetic radiation and visible region with a frequency range of (380-760 Hz) produce a sensation of light. Radiation from the short frequency shows the impression of blue light, radiation with frequencies between 520 nm and 550 nm is seen as a green light, or more around 650 nm we sense the light typically to be of red shading. Addition and subtraction mixing of colour are two main methods to produce colour stimuli. In additive colour mixing lights are mixed, and in subtractive colour mixing, some part is removed from the visible spectrum. It gives the following three important laws:

1. The three autonomous factors are required and adequate to indicate a colour match.
2. The values of tristimulus are more important for the additive mixture of colour stimuli not their spectral compositions.
3. The resulting changes in the values of tristimulus in mixtures when added, color stimuli happen when one or more segments of the mixture keep changing. The perception conditions have been directed: center of the vision, around 3-9 size of field, dull environmental factors; in earlier introduction an adequately long dim adjustment is accepted and the normalized colour-matching functions (CMFs). CMFs have been characterized by finding the average of consequences of many observers. As per Grassman's laws, the 3 selected stimuli (red, green, blue) when added together in a proper proportion can be matched to a colour stimulus. The addition of the 3 stimuli is projected on one side and the sample to be tested its stimulus is projected onto the other side of the field. Through portable light attenuators, the light motion of the three coordinating stimuli is qualified for taking a match of the colours inside the two fields. At the point when this circumstance shows up, the test stimuli can be characterized by the three luminance estimations of the coordinating stimuli arriving at the eye of the observer. There is a difference in the spectral power distributions (SPDs) of the addition of the 3 matching stimuli to that of the test stimulus though they look the same to the human eye but is different. To get the colorimetric framework we need to define both spectral composition and the estimation of amount in units to determine the coordinating stimuli. For a single-color test stimulus, the amounts needed for the colour matching are called CMFs. The addition and multiplication of the sample for many coloured samples are usually done by adding up the colour stimuli.

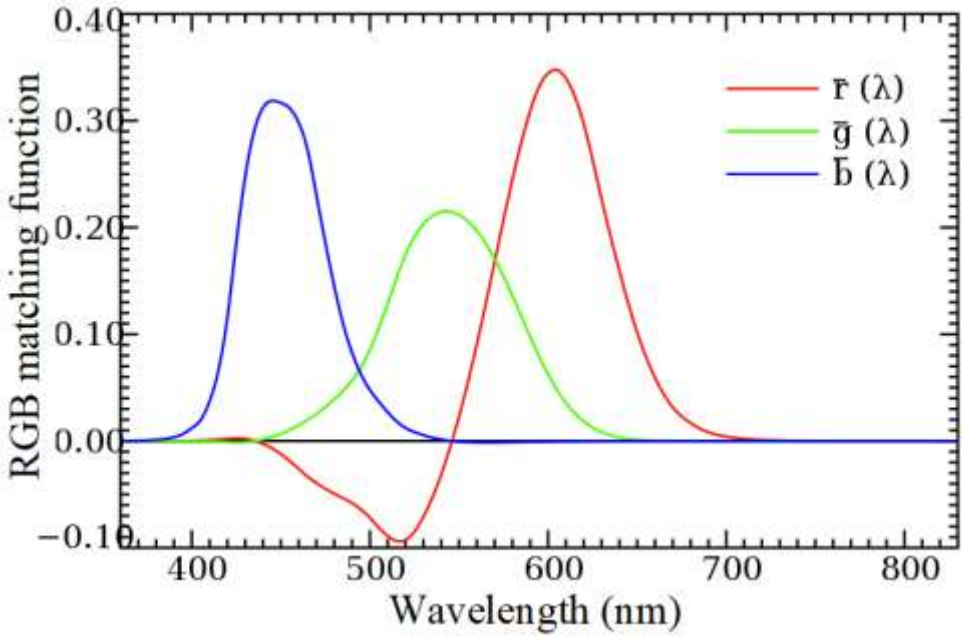

Fig. 1.4: The CIE 1931 RGB Colour matching functions.

The negative lobes in these curves in Fig .1.4.[14], [15] This figure shows if one test stimulus is added to the matching stimuli then only certain parts of the spectrum can be matched. The approximate values of R, G, B was found out by colour stimulus' luminance and units of these 3 primaries are dictated according to luminance. CMFs made calculations more difficult. As a result, the CIE decided in 1931 to transform the real [R], [G], [B] primaries to a set of imaginary primaries [X], [Y], [Z] to avoid negative lobes in CMF. To achieve this, the equienegry tristimulus values should be the same, i.e. X=Y=Z, and photometric quantities should be produced by one of these, whose amount should be minimized.

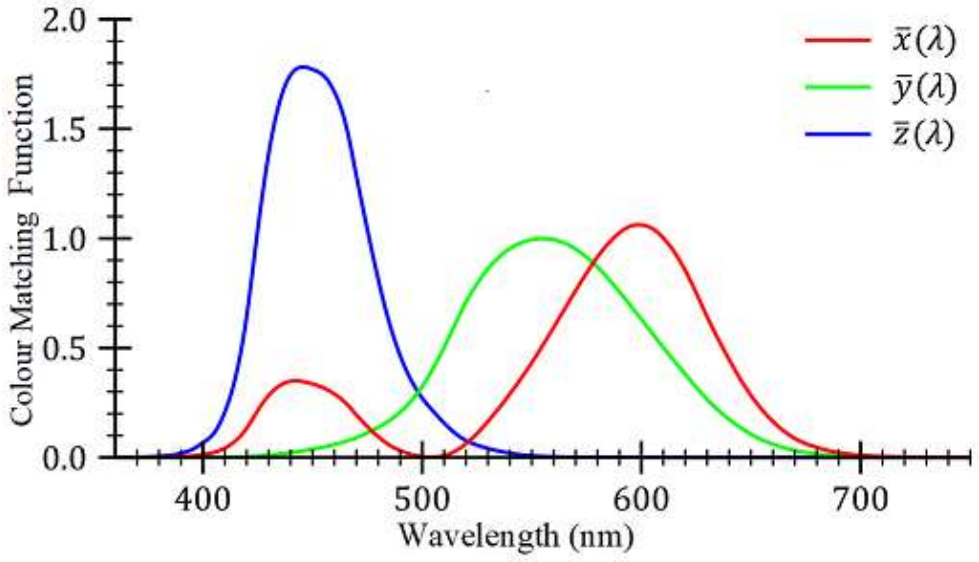

Fig.1.5: CMFs of the CIE 1931 standard colorimetric.

Figure 1.5 indicates the CMFs of the CIE 1931 [16]. According to CIE publication 15, "When more coarsely sampled data produces no significant computation error, selected values from the standard are used 5 nm intervals, Then the calculations will be rounded to 6 decimal places and published in both print and available in electronic form[17].

The colour emitted from rare-earth ion-doped material can be understood through photoluminescence spectra by using CIE.[6],[18] We need these 1-6 following equations to calculate chromaticity coordinates[19]. The Planckian radiator is referred to the black body radiation. The spectral power distribution P(λ ,T) can be calculated by Planck's radiation formula:

$$\boldsymbol{P(\lambda,T) = 2hc^2\lambda^{-5}(\exp\left(\frac{hc}{\lambda k_B T}\right) - 1)^{-1}} \quad \textbf{(1)}$$

Where λ is the wavelength, T is temperature, c is speed of light, h is Planck's constant and K_B is the Boltzmann's constant.

CIE tristimulus is calculated by the following three equations:

$$\boldsymbol{X(T) = k \int P(\lambda,T)\,\bar{x}(\lambda)d\lambda} \quad \textbf{(2)}$$

$$\boldsymbol{Y(T) = k \int P(\lambda,T)\,\bar{y}(\lambda)d\lambda} \quad \textbf{(3)}$$

$$\boldsymbol{Z(T) = k \int P(\lambda,T)\,\bar{z}(\lambda)d\lambda} \quad \textbf{(4)}$$

Where $\bar{x}(\lambda)$, $\bar{y}(\lambda)$ and $\bar{z}(\lambda)$ are the CIE colour matching functions. And X(T), Y(T), and Z(T) are the tristimulus values of CIE 1931.[20],[21] The CIE 1931 chromaticity coordinate is calculated by these two formulae:

$$\mathbf{x} = \frac{\mathbf{X(T)}}{\mathbf{X(T)+Y(T)+Z(T)}} \quad \textbf{(5)}$$

$$\boldsymbol{y} = \frac{\boldsymbol{Y(T)}}{\mathbf{X(T)+Y(T)+Z(T)}} \quad \textbf{(6)}$$

We have calculated CIE chromaticity coordinates from photoluminescence emission spectra by using the above-given formula. The CIE 1931 coordinate system assigns a colour to a point on the chromaticity diagram by using two colour coordinates, x, and y. Fig.1.6 represents the CIE plot[15]. In this figure, the white colour is represented by E point. Similarly, we get information about the emission of colour from material by drawing chromaticity coordinates in CIE plot.

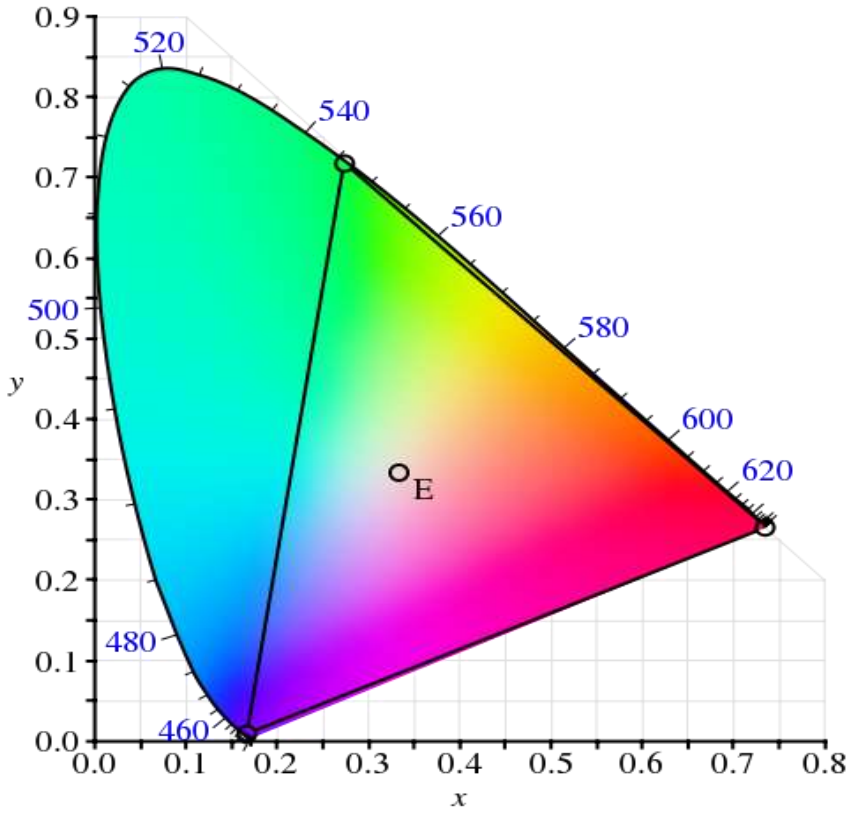

Fig.1.6: Chromaticity diagram of the CIE 1931 plotted on the Cartesian coordinate system.

1.7 Fourier Transform Infrared Spectroscopy

Infrared (IR) spectroscopy is based on the interaction of IR radiation with matter. It is mainly used to identify bonds and functional group that are present in compounds or materials. IR region has wavelength that is higher than visible light, because of which its tendency to induce electronic transitions becomes lower. So, we have three regions in infrared. We have near infrared, mid-infrared and far infrared. In this case, we are talking about mid-infrared region which is essentially 2.5 to 25 μm of wavelength and very often as far as infrared spectroscopy is concerned, the wavelength is referred to by wave number. Now, what is wave number?

$$Wave\ number = \frac{1}{\lambda}$$

Wave number is nothing but just another representation of reciprocal of wavelength. Why is this sort of representation chosen? Because energy is proportional to (1/λ). So, energy in this case is proportional to the wave number. So, range of mid-IR is 4000 cm^{-1} to 400 cm^{-1} corresponds to 2.5 - 25 μm. All molecules that are not going to be active as far as infrared is concerned. If we have homonuclear diatomic molecules like oxygen, hydrogen, nitrogen or chlorine, these will have no response to the radiation because they are going to be inactive as

far as infrared is concerned. Interaction only happens when dipole moment of the molecule changes with vibration - only polar bonds are infrared active and the stronger the polarity in the system, the stronger will be the infrared spectrum that is produced by these materials. We talk about polar. When there is a separation of charges happening between the elements that make up the molecule is polar. For example, water and HCL are polar. There is a separation of charges that happens at the bond and the stronger the difference in polarity, the higher will be the absorption spectrum produced in infrared. When IR radiation interact with polar molecule, they start vibrating because of the different types of vibrations that may actually happen in the molecule. So, since there is a charge imbalance, when send radiation to it, there are different kinds of things that may happen. The bond may start extending or it may start bending or rotating. A lot of different things can happen to the bond because of this absorption of the radiation.

IR spectroscopy simply exploits the fact that molecules have very specific frequencies at which they can rotate or vibrate corresponding to discrete energy levels. For example, Hydrogen and chloride bond and the specific energy that will excite the stretching of this bond, there will be only one single value for that energy that creates this stretching.

IR light is collected on passing it through the sample and how much of the energy that gets absorbed or transmitted can give an indication of specific wavelengths at which induce vibrations happening in the system. We have seen several systems; we saw that there is a need to actually isolate the wavelengths to send them through the sample. In the case of UV-visible spectrometers, we talked about the array-detectors in which all wavelengths collect together at the same time. Similarly, in the case of Fourier transform, to make the technique a lot more robust, either we can use a monochromatic beam, which changes in wavelength over time, and collect all the wavelengths together and do a Fourier transform, to measure all the wavelengths at once. So that is why today, what we typically call IR spectroscopy is FTIR spectroscopy or Fourier Transform Infrared Spectroscopy. The idea is that you can isolate all the frequencies or all the wavelengths at once, rather than having to individually choose wavelengths of infrared light to be passed through the sample. Cooley and Tukey discovered the Fast Fourier Transform (FFT) algorithm.[22] In which the number of necessary computations is drastically reduced when compared to the classical Fourier transform. This algorithm is generally used in FTIR instrument to overcome complexity in calculation. In the FTIR spectrum, we plot the absorbance or the transmittance on the Y-axis and the wavelength on the X-axis, but in this

case, we do not plot the wavelength, we plot the wave number. So, we plot the wave number on the X-axis and the % absorbance or % transmittance.

Typical IR absorption wavelengths are divided into 2 groups, one is called the fingerprint region (1500-400 cm^{-1}), the other is called the functional group region (4000-1500cm^{-1}). At the higher end of the absorption spectra, that means at higher wave numbers is called functional group regions. For example, nitrogen-hydrogen (N-H) group, alcohol group (O-H) and so on. These are essentially the functional groups that may be present in the systems. On the other hand, when you go towards the lower end of the wave number, what you get is the fingerprint, which essentially corresponds to the presence of single bond, double bond or triple bonded systems. Based on the specific sets of wave numbers at which you get these transitions, we can approximately estimate the composition and structure of the material.

We will need to compare with the database to try and understand what each peak signifies. For most of the standard bonding systems like C≡C or C=C, there are very specific locations at which transitions happen like stretching or bending and so on and the associate peaks that we observe for our sample and then figure out what actually is present in the sample.

Figure 1.7 shows the how spectra is produced. First of all we have the light source. This light then passes through an instrument called the interferometer. The interferometer essentially brings out light rays that are either completely in phase or out of phase based on the movement of some mirrors, which are inside the interferometer. This light that comes out of the interferometer, then passes through the sample and creates what is known as an interferogram, and this interferogram is then subjected to the Fourier transform process. Fourier transform is simply mathematical technique for separating the frequency components of a complicated wave[23]. We are operating at infrared wavelengths, so, there is sufficient amount of infrared radiation in the background also which needs to be removed from the system to actually get a clear understanding of the absorbance spectra for the sample itself and ultimately get transmission spectrum. And the percentage transmittance is plotted against the wave number on the X-axis and get FTIR spectra.

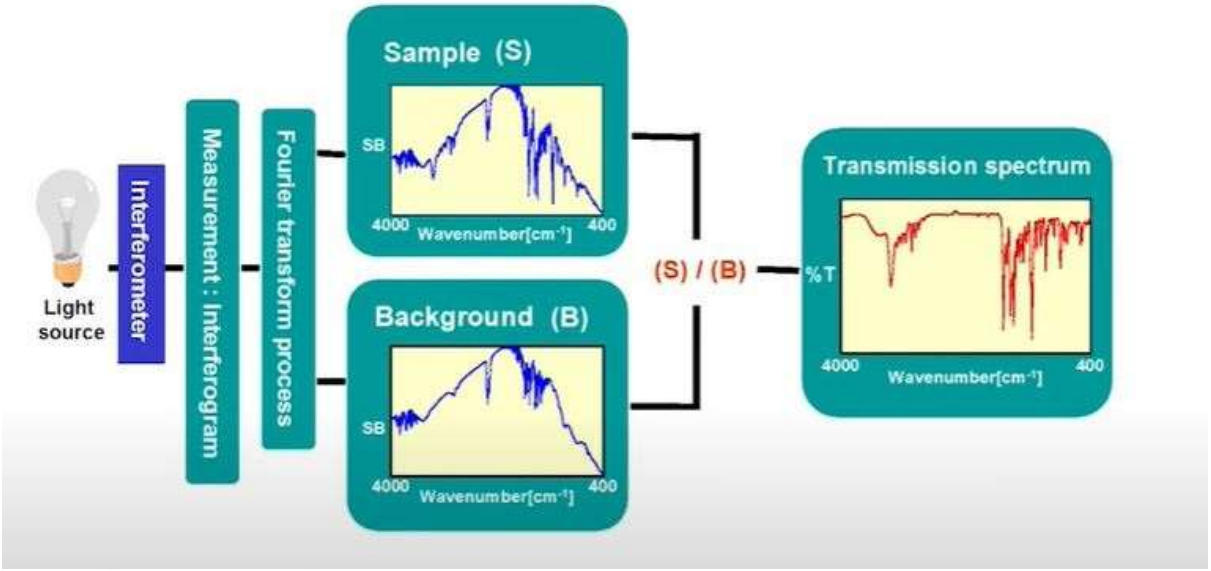

Fig.1.7: FTIR flow chart.

CHAPTER 2

EXPERIMENTAL WORK

2.1 Synthesis

Melt Quench Method

It is the most common method used in the preparation of glass. It was the first technique used in the industry of glass and in research field. The other two methods used for the preparation of glass are chemical vapour deposition (CVD) and sol gel technique. A large number of borate, silicate, phosphate and oxide glasses can be manufactured using melt quenching method. Glass can be easily doped with active ions by using this technique. The disadvantage of using this method is lack of purity of prepared glass. To avoid the impurity, Gold and Platinum based crucibles are used in research laboratories.

Reagents

The solid reactants from which is used in the formation of the phosphors or any crystalline compound. The reactant chemicals used in it depends on the feasibility to use, some reaction conditions and final product.

Mixing

After the reactants have been weighed according to their stoichiometric ratios in the chemical equation, they are mixed. Acetone or alcohol are some of the volatile organic liquid which is sufficiently added in the mixture to get an equal mix of all the reactants used. Paste type mixture is formed which is grinded thoroughly till the organic liquid volatilizes and evaporated completely about in 10-15 min to again get powder like compound.

Container material

Subsequent reaction at high temperatures takes place in furnace. The container in which the grinded powder is put to be kept in the furnace needs to be chemically inert to the powder when heated at such high temperature.

Sample Preparation

Sm^{3+}doped borosilicate (BSAC: xSm) glass was prepared by classical melt quench process with the following compounds composition: $50B_2O_3$-$20SiO_2$-$15Al_2O_3$(15-x)CaO-xSm_2O_3 (where x = 0.1, 0.5, 1.0, 1.5 & 2.0 mol%). It was synthesized by using H_3BO_3, SiO_2, Al_2O_3, CaO, and Sm_2O_3 chemical constituents as main compounds. All these aforementioned chemical constituents were mixed with acetone and crushed all together for 30 minutes in a agate mortar until to get the smooth powder and then transferred into the crucible. Thereafter the crucible was placed inside the muffle furnace and heated it at 1250ºC for one hour. The Mixed powder was melted then quickly quenched with the help of pre-heated brass plates and three coins to make a glass sample of uniform thickness. Thereafter, put it in another electric furnace at 350ºC for about 2 hours to avoid the thermal strains, air bubbles from the as-prepared glass. Finally, the Sm^{3+} doped borosilicate glass sample is prepared to study their novel properties. The image of all synthesized glasses are shown in Figure 2.1.

Fig. 2.3. Image of the synthesized glasses.

2.2 Analysis of sample

The XRD profile of synthesized host glass was observed by a X-ray Bruker D8 Advance Diffractometer. In this instrument, X-ray is generated by Cu-Kα radiation (λ=1.54Å). PL emission and excitation were monitored by Jasco FP-8300 spectrofluorometer. The photoluminescence decay spectral information was recorded by using an Edinburgh FL920 Fluorescence Lifetime Spectrometer. The FT-IR spectrum was monitored via Spectrum Two FT-IR Spectrometer- PerkinElmer.

CHAPTER 3

RESULTS AND DISCUSSION

3.1 XRD analysis:

Fig. 2 depicts the XRD spectrum of the as-synthesized host glass sample. It was monitored in the 2Ɵ range from 10 to 70 degrees. It clearly differentiates the crystalline and amorphous nature of glass. No distinguishable intense peaks were observed in Fig.3.1, but a wide-ranging hump has been observed at low scattering angles, which specifies the glassy nature of prepared borosilicate glasses.

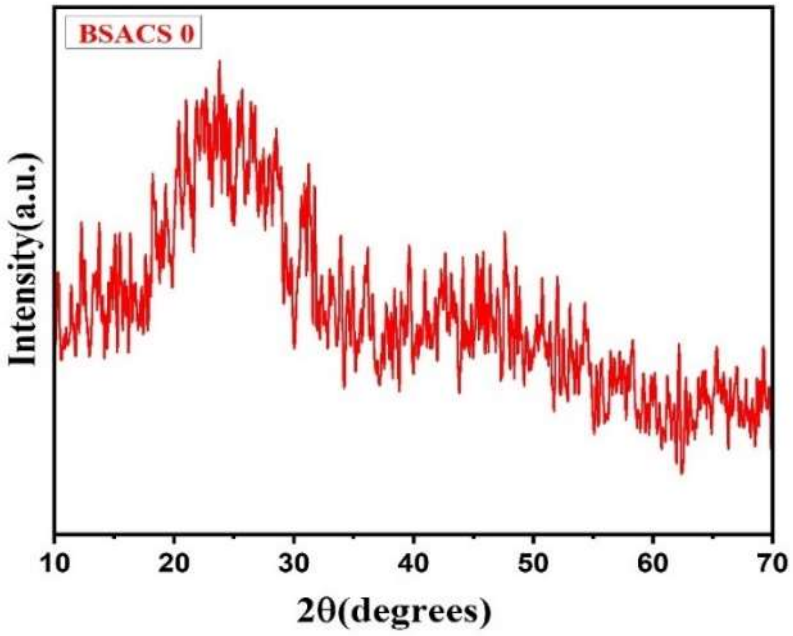

Fig. 3.1. XRD profile of un-doped borosilicate glass.

3.2 Photoluminescence excitation and emission spectral studies:

The excitation spectrum was recorded from 300 to 500 nm under a fixed emission wavelength at 599nm. Fig. 3.1 shows the information pertaining to the excitation spectrum recorded for (0.5mol%) Samarium ions doped as-prepared glass; it confirms the presence of many excitation peaks in the orange region. The details of excitation bands observed at different wavelengths corresponding to the transitions are shown in the Table 3.1 [6],[24]–[26].

Table 3.4. The excitation peaks and their corresponding wavelength.

The transition from $^6H_{5/2}\rightarrow$	**The excitation bands are centered at the wavelength (λ)**
$^4H_{9/2}$	343
$^4D_{3/2}$	360
$^6P_{7/2}$	374
$^4F_{7/2}$	402
$^6M_{19/2}$	416
$^4G_{9/2}$	437
$^4I_{11/2}$	473

After analyzing the excitation spectrum, we found that amongst all peaks, the transition $^6H_{5/2} \rightarrow {}^4F_{7/2}$ (402 nm) shows maximum intensity. The blue spectrum ranging from 500 to 750 nm in Figure 3.2, depicts the emission profile of as prepared glass (0.5 mol %) near-UV excitation.

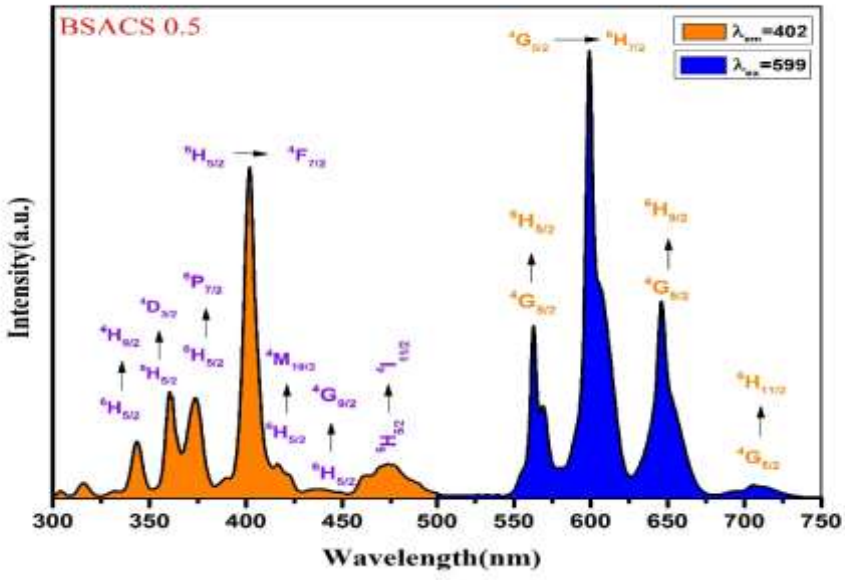

Fig. 4.2. PL excitation and emission profile of 0.5 mol% Sm^{3+} doped as prepared borosilicate glass.

The emission spectrum contains four peaks centered at different wavelengths corresponding to the transitions are shown in Table 2.

Table 3.5. The emission peaks are centered at wavelength corresponding to the transitions

The transition from $^4G_{5/2}\rightarrow$	**The excitation bands are centered at the wavelength (λ)**
$^6H_{5/2}$	562
$^6H_{7/2}$	599
$^6H_{9/2}$	646
$^6H_{11/2}$	702

After analyzing the emission spectrum, we found that amongst all four peaks, the transition $^4G_{5/2} \rightarrow {}^6H_{7/2}$ (599 nm) shows the maximum intense peak and found in the reddish-orange region.

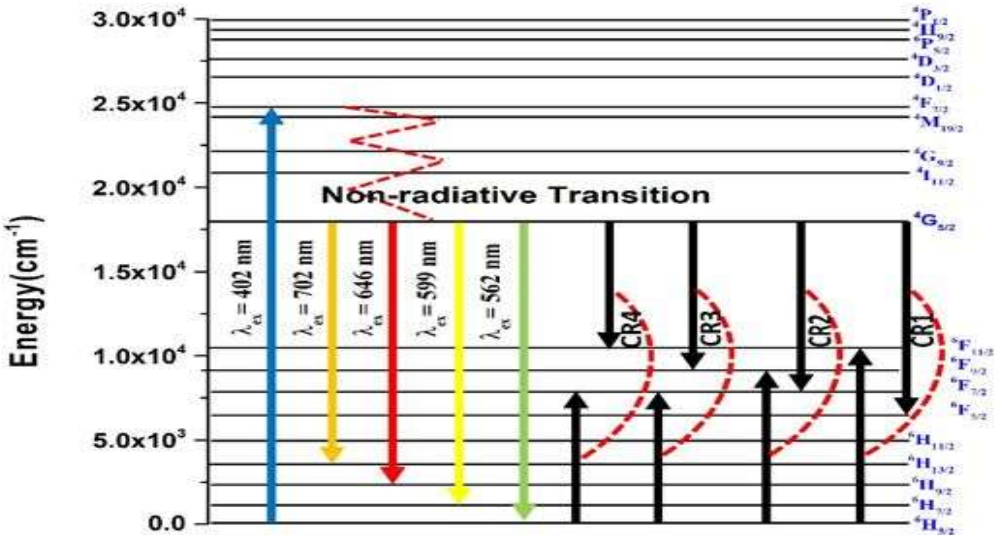

Fig. 3.3. Energy level diagram of the prepared glass.

Figure 3.3 depicts the energy levels of Samarium ions doped borosilicate glasses. The solid lines denote the radiative transitions and the dashed lines are representing the non-radiative transitions. Due to the minimal energy difference, all excitation thresholds above 4G5/2 undergo non-radiative relaxation to this state. The radiative (visible) transitions which are taking place from 4G5/2 to different energy states of 6Hj (j=5/2, 7/2, 9/2 & 11/2) are because there is enough energy gap between them. Because of the small energy gap between closest energy levels, non-radiative transitions occur [6].

3.3 FT-IR spectral analysis:

A pellet of thickness 1 mm is prepared by compressing the mixture of KBr and glass powder in a hydraulic press under high pressure. This pellet is used in a spectrometer to obtain the FT-IR spectra. FT-IR spectrum of host glass is shown in Figure 3.4. we get the information of the molecular or rotational vibrations associated with the bonds from FT-IR spectra. The obtained bands are located at 702, 944, 1045, 1088, 1146, 1298, 1339, 1394, and 1498 cm^{-1} respectively. This figure also contains two broad bands ranging from 2700-3000 cm^{-1} and 3600-3750 cm^{-1}. The band positions and their assigned modes of vibrations present in the glass are presented in Table 3.3.

Table 3.6. FT-IR band assignments for the glass sample BSAC: xSm^{3+} (x = 0 mol%)

Peak Positions Wavenumbers (cm−1)	**Assignments**	**References**
3600–3750	OH Water	[27]
2700–3000	Hydrogen bonding	[28][29]
~1498	Three nonbridging oxygens of the B–O–B groups produce anti-symmetric stretching vibrations.	[30]
~1394	B–O asymmetric vibrations in BO_3^- and BO_2O^- units	[31], [32]
~1339	B–O stretching vibrations of pyroborate, meta, and orthoborate groups	[28], [30]
~1298	Symmetric stretching vibration of B–O in $BO_3^{-`}$	[30], [33]
~1146	B-O stretching vibrations of trigonal $BO_3^{-`}$ units only	[31]
~1088	Asymmetric stretching vibration of Si–O–Si bonds	[34], [35]
~1045	B–O Stretching vibration of tetrahedral $BO_4^{-`}$ unit	[28]
~944	Stretching vibration of Si-OH	[36]
~702	B–O–B vibrations in the borate networks	[37],[38]

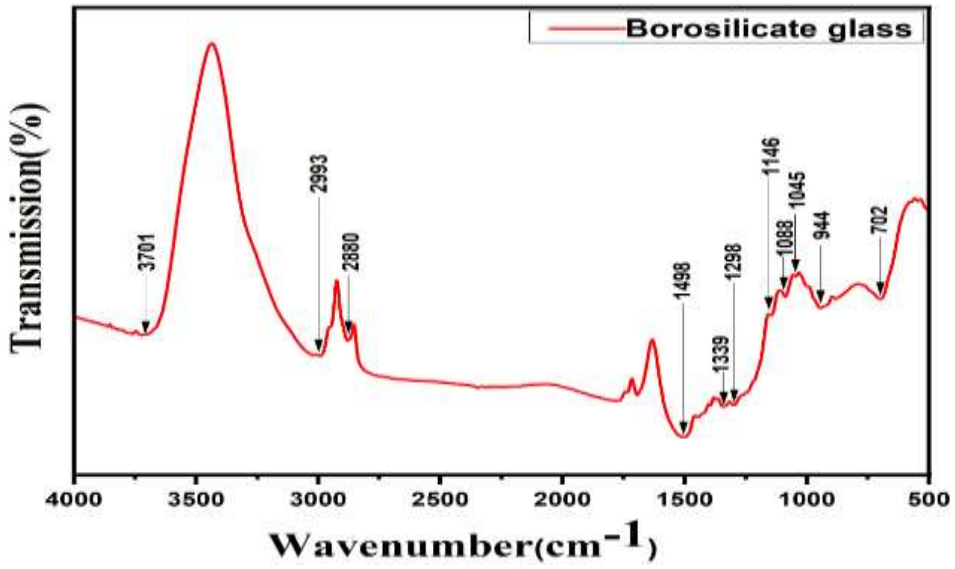

Fig. 3.4. FT-IR profile of un-doped borosilicate glass.

3.4 Photoluminescence lifetime decay curve analysis:

PL decay profiles were monitored at 599nm emission wavelength under 402nm excitation wavelength. The measured results are depicted in Figure 3.5. The PL decay profiles were plotted in a semi-logarithmic plot and normalized on the maximum intensity. The PL decay curve recorded for BSAC: xSm3+(0.1) was fitted using bi-exponential function:[39]

$$\boldsymbol{I(t) = A_1 exp\left(-\frac{t}{\tau_1}\right) + A_2 exp(-\frac{t}{\tau_2})} \qquad (1)$$

and PL decay curve recorded for BSAC: xSm3+ (0.5 & 1.5) were fitted by using the tri-exponential function:

$$\boldsymbol{I(t) = A_1 exp\left(-\frac{t}{\tau_1}\right) + A_2 exp\left(-\frac{t}{\tau_2}\right) + A_3 exp(-\frac{t}{\tau_3})} \qquad (2)$$

In which constants have their usual meanings. The average decay lifetime τ can be determined by:

$$\boldsymbol{\tau = \frac{A_1(\tau_1)^2 + A_2(\tau_2)^2 + A_3(\tau_3)^2}{A_1\tau_1 + A_2\tau_2 + A_3\tau_3}} \qquad (3)$$

The photoluminescence decay profile of Sm^{3+} doped borosilicate glass is depicted in Figure 3.5, In which glass with concentration 0.1 mol% is fitted bi-exponentially and the other two are fitted tri-exponentially [40]. The average decay time (τ_{avg}) of BSAC: xSm^{3+} (x=0.1, 0.5 and 1.5 mol %) is 2.85 µs, 1.86 µs and 1.36 µs respectively. τ_{avg} of the glasses decrease quickly

after increasing the dopant ion concentrations and this happens because of the transfer of energy between Samarium ions at smaller distances.

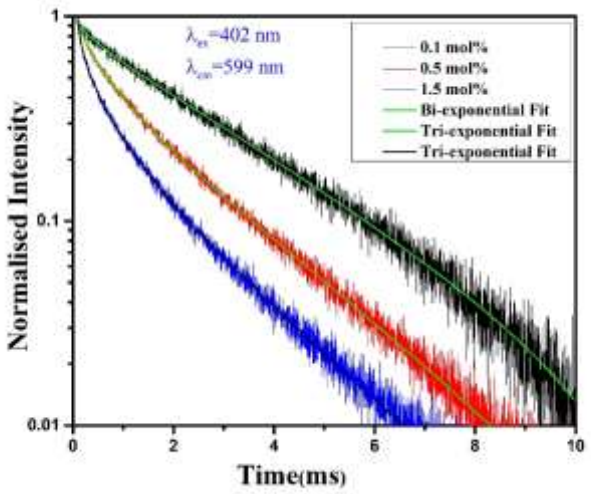

Fig. 3.5. Photoluminescence decay profile of BSAC: xSm^{3+}(x = 0.1, 0.5, 1.5) samples under 402 nm excitation, monitoring emission at 599 nm.

3.5 CIE chromaticity coordinates:

The calculated CIE chromaticity coordinates of the Sm+3 doped glass from emission spectra are shown in Table 3.4. The CIE 1931 coordinate system assigns a colour to a point on the chromaticity diagram by using two colour coordinates, x, and y. CIE plot with chromaticity coordinates is shown in Figure 3.6. In this figure, clearly we can see that, coordinates are positioned in reddish-orange region in CIE plot. This shows that this material can be used in reddish-orange luminescent device applications.

Table 3.7. The color coordinates of CIE diagram.

Glass sample doping concentration Mol %	**Colour Coordinates**	
	X	**Y**
0.1	0.5842	0.3958
0.5	0.5998	0.3964
1.0	0.5934	0.4005
1.5	0.5871	0.3979
2.0	0.5930	0.4019

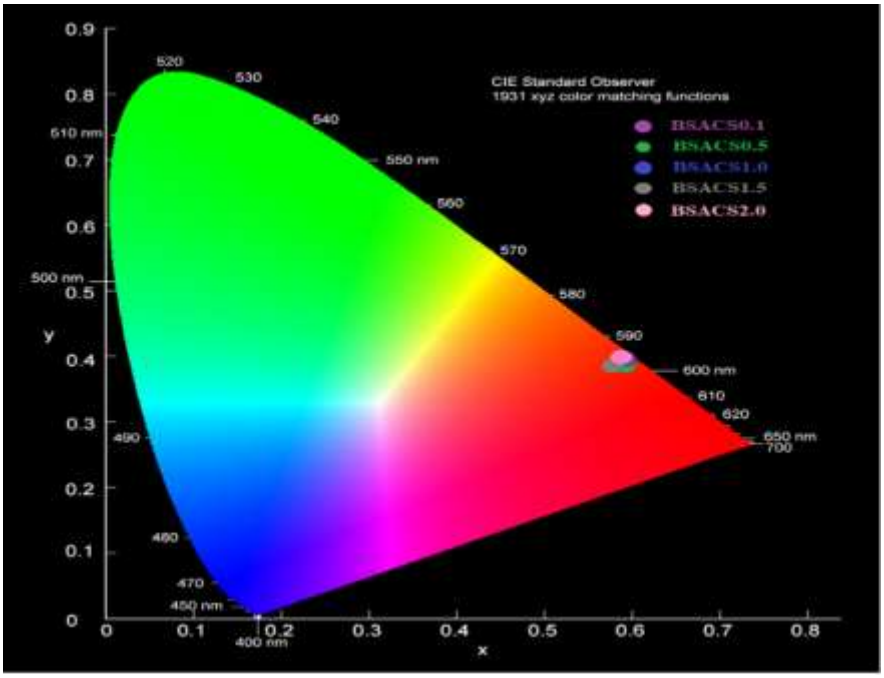

Fig. 3.6. CIE diagram of Sm^{+3} doped borosilicate glasses.

CHAPTER 4

CONCLUSION

Borosilicate (BSAC: xSm^{3+}) glasses doped with Samarium ions were developed by using melt quench method. Borosilicate glasses are characterized by using XRD, FT-IR, photoluminescence excitation, emission, and PL decay spectral studies to comprehend the use of these materials in photonic device applications. The XRD and FT-IR studies of the host glass sample tells about the amorphous nature and presence of different bonds and functional groups. The most intense peak ($^4G_{5/2} \rightarrow {}^6H_{7/2}$) is centered at 599nm in the PL profile. The experimental lifetime decreases as doping ion concentration increases and this happens because of the non-radiating transition that takes place between borosilicate glass and Sm^{3+} ions. The coordinates of CIE obtained for an optimum concentration of doping ion in borosilicate (BSAC: xSm^{3+}) glasses are 0.561, 0.435, where x=0.5 mol %. All of the above findings indicate that Sm^{3+} doped borosilicate glass is suitable for its usage in visible reddish orange photonic devices.

Reference

[1] N. Deopa and A. S. Rao, "Spectroscopic studies of Sm3+ ions activated lithium lead alumino borate glasses for visible luminescent device applications," *Optical Materials*, vol. 72, pp. 31–39, 2017, doi: 10.1016/j.optmat.2017.04.067.

[2] S. Mahamuda, K. Swapna, M. Venkateswarlu, A. Srinivasa Rao, S. Shakya, and G. Vijaya Prakash, "Spectral characterisation of Sm3+ ions doped Oxy-fluoroborate glasses for visible orange luminescent applications," *Journal of Luminescence*, vol. 154, pp. 410–424, 2014, doi: 10.1016/j.jlumin.2014.05.017.

[3] N. Deopa, S. Kaur, A. Prasad, B. Joshi, and A. S. Rao, "Spectral studies of Eu3+ doped lithium lead alumino borate glasses for visible photonic applications," *Optics and Laser Technology*, vol. 108, pp. 434–440, 2018, doi: 10.1016/j.optlastec.2018.07.010.

[4] Q. Chen, Q. Chen, and M. Ferraris, "Effect of Ceramic Crucibles on Magneto-Optical PbO-Bi₂O₃-B₂O₃Glasses Properties," *New Journal of Glass and Ceramics*, vol. 02, no. 01, pp. 41–50, 2012, doi: 10.4236/njgc.2012.21007.

[5] A. Ghosh and B. K. Chaudhuri, "Preparation and characterization of binary V2O5-Bi2O3 glasses," *Journal of Materials Science*, vol. 22, no. 7, pp. 2369–2376, 1987, doi: 10.1007/BF01082118.

[6] N. Deopa, B. Kumar, M. K. Sahu, P. R. Rani, and A. S. Rao, "Effect of Sm 3+ ions concentration on borosilicate glasses for reddish orange luminescent device applications," *Journal of Non-Crystalline Solids*, vol. 513, no. January, pp. 152–158, 2019, doi: 10.1016/j.jnoncrysol.2019.03.025.

[7] R. S. Quimby, P. A. Tick, N. F. Borrelli, and L. K. Cornelius, "Quantum efficiency of Pr3+ doped transparent glass ceramics," *Journal of Applied Physics*, vol. 83, no. 3, pp. 1649–1653, 1998, doi: 10.1063/1.366879.

[8] R. Van Deun, K. Binnemans, C. Görller-Walrand, and J. L. Adam, "Judd-Ofelt intensity parameters of trivalent lanthanide ions in a NaPO3-BaF2 based fluorophosphate glass," *Journal of Alloys and Compounds*, vol. 283, no. 1–2, pp. 59–65, 1999, doi: 10.1016/S0925-8388(98)00895-0.

[9] O. Ravi, C. Madhukar Reddy, L. Manoj, and B. Deva Prasad Raju, "Structural and optical studies of Sm3+ ions doped niobium borotellurite glasses," *Journal of Molecular Structure*, vol. 1029, pp. 53–59, 2012, doi: 10.1016/j.molstruc.2012.06.059.

[10] V. Venkatramu, P. Babu, C. K. Jayasankar, T. Tröster, W. Sievers, and G. Wortmann, "Optical spectroscopy of Sm3+ ions in phosphate and fluorophosphate glasses," *Optical Materials*, vol. 29, no. 11, pp. 1429–1439, 2007, doi: 10.1016/j.optmat.2006.06.011.

[11] K. Swapna, S. Mahamuda, A. S. Rao, T. Sasikala, and L. R. Moorthy, "Visible luminescence characteristics of Sm3+ doped Zinc Alumino Bismuth Borate glasses,"

Journal of Luminescence, vol. 146, pp. 288–294, 2014, doi: 10.1016/j.jlumin.2013.09.035.

[12] K. K. Mahato, D. K. Rai, and S. B. Rai, "Optical studies of Sm3+ doped oxyfluoroborate glass," *Solid State Communications*, vol. 108, no. 9, pp. 671–676, 1998, doi: 10.1016/S0038-1098(98)00442-6.

[13] E. Spectroscopy, "Colorimetry , Theory," no. January, pp. 337–343, 2000.

[14] V. E. Johansen, J. Andkjær, and O. Sigmund, "Design of structurally colored surfaces based on scalar diffraction theory," *Journal of the Optical Society of America B*, vol. 31, no. 2, p. 207, 2014, doi: 10.1364/josab.31.000207.

[15] R. Vardasca and J. Gabriel, "A proposal of a standard rainbow false color scale for thermal medical images," pp. 1–5.

[16] M. Amara, F. Mandorlo, R. Couderc, F. Gérenton, and M. Lemiti, "Temperature and color management of silicon solar cells for building integrated photovoltaic," *EPJ Photovoltaics*, vol. 9, pp. 1–11, 2018, doi: 10.1051/epjpv/2017008.

[17] F. Grum, R. F. Witzel, and P. Stensby, "Evaluation of Whiteness.," *J Opt Soc Am*, vol. 64, no. 2, pp. 210–215, 1974, doi: 10.1364/JOSA.64.000210.

[18] C. S. McCamy, "Correlated color temperature as an explicit function of chromaticity coordinates," *Color Research & Application*, vol. 17, no. 2, pp. 142–144, 1992, doi: 10.1002/col.5080170211.

[19] A. R. Robertson, "Computation of Correlated Color Temperature and Distribution Temperature," *Journal of the Optical Society of America*, vol. 58, no. 11, pp. 1528–1535, 1968.

[20] D. B. Judd, "The 1931 I C I Standard Observer and Coordinate System for Colorimetrya,b," *Journal of the Optical Society of America*, vol. 23, no. 10, p. 359, 1933, doi: 10.1364/josa.23.000359.

[21] C. Li *et al.*, "Accurate method for computing correlated color temperature," *Optics Express*, vol. 24, no. 13, p. 14066, 2016, doi: 10.1364/oe.24.014066.

[22] "Cooley65.pdf." .

[23] P. Murugasen, S. Sagadevan, and D. Shajan, "Preparation, techniques and tools used for investigating glasses: An overview," *International Journal of Chemical Sciences*, vol. 13, no. 2, pp. 693–713, 2015.

[24] Q. Xu, D. Xu, and J. Sun, "Preparation and luminescence properties of orange-red Ba3Y(PO4)3:Sm3+ phosphors," *Optical Materials*, vol. 42, pp. 210–214, 2015, doi: 10.1016/j.optmat.2014.12.035.

[25] D. Tu, Y. Liang, R. Liu, Z. Cheng, F. Yang, and W. Yang, "Photoluminescent properties of LiSrxBa1-xPO 4:RE3+ (RE = Sm3+, Eu3+) f-f transition phosphors," *Journal of Alloys and Compounds*, vol. 509, no. 18, pp. 5596–5599, 2011, doi:

10.1016/j.jallcom.2011.02.077.

[26] G. Seeta Rama Raju, J. S. Yu, J. Y. Park, H. C. Jung, and B. K. Moon, "Photoluminescence and cathodoluminescence properties of nanocrystalline Ca 2Gd 8Si 6O 26: Sm 3+ phosphors," *Journal of the American Ceramic Society*, vol. 95, no. 1, pp. 238–242, 2012, doi: 10.1111/j.1551-2916.2011.04762.x.

[27] T. A. Taha and A. S. Abouhaswa, "Preparation and optical properties of borate glass doped with MnO2," *Journal of Materials Science: Materials in Electronics*, vol. 29, no. 10, pp. 8100–8106, 2018, doi: 10.1007/s10854-018-8816-7.

[28] C. Gautam, A. K. Yadav, and A. K. Singh, "A Review on Infrared Spectroscopy of Borate Glasses with Effects of Different Additives," *ISRN Ceramics*, vol. 2012, pp. 1–17, 2012, doi: 10.5402/2012/428497.

[29] K. Marimuthu, R. T. Karunakaran, S. Surendra Babu, G. Muralidharan, S. Arumugam, and C. K. Jayasankar, "Structural and spectroscopic investigations on Eu3+-doped alkali fluoroborate glasses," *Solid State Sciences*, vol. 11, no. 7, pp. 1297–1302, 2009, doi: 10.1016/j.solidstatesciences.2009.04.011.

[30] P. P. Pawar, S. R. Munishwar, and R. S. Gedam, "Physical and optical properties of Dy3+/Pr3+ Co-doped lithium borate glasses for W-LED," *Journal of Alloys and Compounds*, vol. 660, pp. 347–355, 2016, doi: 10.1016/j.jallcom.2015.11.087.

[31] M. R. Ahmed and M. Shareefuddin, "EPR, optical, physical and structural studies of strontium alumino-borate glasses containing Cu2+ ions," *SN Applied Sciences*, vol. 1, no. 3, 2019, doi: 10.1007/s42452-019-0201-5.

[32] T. A. Taha and A. S. Abouhaswa, "Preparation and optical properties of borate glass doped with MnO2," *Journal of Materials Science: Materials in Electronics*, vol. 29, no. 10, pp. 8100–8106, 2018, doi: 10.1007/s10854-018-8816-7.

[33] I. Ardelean, S. Cora, and D. Rusu, "EPR and FT-IR spectroscopic studies of Bi2O3- B 2O3- CuO glasses," *Physica B: Condensed Matter*, vol. 403, no. 19–20, pp. 3682–3685, 2008, doi: 10.1016/j.physb.2008.06.016.

[34] T. Xiu, Q. Liu, and J. Wang, "Alkali-free borosilicate glasses with wormhole-like mesopores," *Journal of Materials Chemistry*, vol. 16, no. 41, pp. 4022–4024, 2006, doi: 10.1039/b612215a.

[35] G. Shao *et al.*, "Thermal shock behavior and infrared radiation property of integrative insulations consisting of MoSi2/borosilicate glass coating and fibrous ZrO2 ceramic substrate," *Surface and Coatings Technology*, vol. 270, no. May 2015, pp. 154–163, 2015, doi: 10.1016/j.surfcoat.2015.03.008.

[36] S. T. Wang, M. L. Chen, and Y. Q. Feng, "A meso-macroporous borosilicate monolith prepared by a sol-gel method," *Microporous and Mesoporous Materials*, vol. 151, pp. 250–254, 2012, doi: 10.1016/j.micromeso.2011.10.029.

[37] M. Diantoro, N. D. Prastiwi, A. Taufiq, N. Hidayat, N. Mufti, and A. Hidayat, "The Role of Fe2O3 and Light Induced on Dielectric Properties of Borosilicate Glass," *Journal of Physics: Conference Series*, vol. 846, no. 1, pp. 1–6, 2017, doi: 10.1088/1742-6596/846/1/012007.

[38] A. A. Alemi, H. Sedghi, A. R. Mirmohseni, and V. Golsanamlu, "Synthesis and characterization of cadmium doped lead-borate glasses," *Bulletin of Materials Science*, vol. 29, no. 1, pp. 55–58, 2006, doi: 10.1007/BF02709356.

[39] D. Wang, P. Zhang, Q. Ma, J. Zhang, and Y. Wang, "Synthesis, optical properties and application of Y 7 O 6 F 9 :Er 3+ for sensing the chip temperature of a light emitting diode," *Journal of Materials Chemistry C*, vol. 6, no. 48, pp. 13352–13358, 2018, doi: 10.1039/c8tc05307c.

[40] G. Swati *et al.*, "Investigation on luminescence enhancement and decay characteristics of long afterglow nanophosphors for dark-vision display applications," *Applied Surface Science*, vol. 333, pp. 178–185, 2015, doi: 10.1016/j.apsusc.2015.01.135.

Sm^{3+} ions doped Borosilicate glasses for visible photonic device applications

Ashish Makhloga, Videsh Kumar and A.S.Rao*

Department of Applied Physics, Delhi Technological University, Bawana Road, New Delhi-110042

Abstract. An intense reddish-orange colour radiating Samarium doped Aluminium Calcium borosilicate (BSACS) glasses were synthesized by the melt-quench method to analyze the photoluminescence properties using characterization methods like XRD, FT-IR, photoluminescence (PL) excitation, PL emission, and PL decay. XRD and FT-IR reveal the non-crystalline behavior along with the presence of numerous functional groups in BSACS host glass correspondingly. Under 402 nm excitation, three major peaks were found in the emission spectra which perfectly resembles to $^4G_{5/2} \rightarrow {}^6H_{5/2}$ (562 nm), $^4G_{5/2} \rightarrow {}^6H_{7/2}$ (599 nm), $^4G_{5/2} \rightarrow {}^6H_{9/2}$ (646 nm) and $^4G_{5/2} \rightarrow {}^6H_{9/2}$ (702 nm) transitions of Samarium ions. $^4G_{5/2} \rightarrow {}^6H_{7/2}$ transition at 599 nm is comparatively more intense and noticeable. PL decay observed for $^4G_{5/2}$ state reveals the exponential nature in which curves are fitted by using bi-exponential and tri- exponential fitting to assess the practically measured lifetimes (τ_{exp}). It is observed that the τ_{exp} values are decreasing with increasing Samarium ion concentration due to cross-relaxation energy transference. All of the findings indicate that Sm^{3+} doped borosilicate glass is suitable for its usage in visible reddish-orange photonic devices.

Keywords: Borosilicate glasses, Samarium ion, FT-IR, Photoluminescence, CIE coordinates, Photoluminescence decay.

*Corresponding author: E-mail: drsrallam@gmail.com (Prof. A.S. Rao), Tel: +91 85860 39007, Fax: +91 01127871023

1. Introduction

Modern technology linked to optical devices have seen the usage of rare earth (RE) ions doped oxide glasses. They are used in large number of applications and these are much important for the advancement of different types of optoelectronic devices like display screens, waveguides, solid-state laser, reflecting windows and sensors, etc. To achieve optimum output and optimized properties, two approaches are commonly used for RE-based glasses: (a) by altering the host materials composition/active ion concentration (RE ion) and (b) by altering its geometrical design through applying external pressure around RE ion. In the current study, the prior approach has been followed to

study the photoluminescence (PL) property of borosilicate glass doped with Sm^{3+} ion in different concentrations. In addition, from different types of RE ion, Samarium ions are effective in generating red-orange light in the visible region. And the different types of glass give the strong fluorescence which makes it very significant for luminescent devices.

Boron trioxide (B_2O_3) plays a significant role in the glass formation attributable to its high thermally stable, high transparency, low freezing point, high RE ions solubility [1], [2]. On the other hand, Boron trioxide in glasses alone possesses high phonon energy ($1300cm^{-1}$) because of the stretching vibrations of network-forming oxides [3]. Non-radiating transitions are mainly enhanced in the presence of high phonon energies, which significantly reduce the RE ion emissions. An oxide of heavy metal such as Al_2O_3 cannot act as a conventional glass former because of its small field strength and high polarizability. However, it may be built a network pyramid within the presence of oxides like B_2O_3 and SiO_2 [4]–[6]. The alkaline earth oxides for example barium, calcium, strontium, and magnesium can change the energy state so photosensitive properties of the host glass also can be changed. Sm^{3+} ions have been widely studied spectroscopically to characterize them for optoelectronic devices and other applications [7]–[9]. Sm^{3+} ion radiates the energy in the visible region from a higher energy excited state to lower energy states via emission with the high quantum efficiency [10]. Sm^{3+} ions are a fascinating case for studying the energy transfer process [11]. The visible fluorescence of the Sm^{3+} ion with the $4f^5$ configuration is strong reddish-orange, and is useful in applications such as optical storage devices, underwater communication, laser devices, and color displays [12].

Recently, Nisha Deopa et al. have studied the structural and luminous nature of Sm^{3+} doped borosilicate glass and confirm the emission of the reddish-orange color under the excitation wavelength 403 nm [6]. These kinds of glasses can be used in photonic device applications [6]. In this research article, the effect on photosensitive properties of borosilicate glasses due to different concentrations of samarium ion are discussed. Further, RE ions doped borosilicate glasses were investigated and we have presented the optical, structural properties, and energy transfer characteristics.

2. Experimental

Sm^{3+}doped borosilicate (BSAC:xSm) glass was prepared by classical melt quench process with the following compounds composition: $50B_2O_3$-$20SiO_2$-$15Al_2O_3$(15-x)CaO-xSm_2O_3 (where x = 0.1, 0.5, 1.0, 1.5 & 2.0 mol%). It was synthesized by using H_3BO_3, SiO_2, Al_2O_3, CaO, and Sm_2O_3 chemical constituents as main compounds. All these aforementioned chemical constituents were mixed with acetone and crushed all together for 30 minutes in a agate mortar until to get the smooth powder and then transferred into the crucible. Thereafter the crucible was placed inside the muffle furnace and heated it at 1250°C for one hour. The Mixed powder was melted then quickly quenched with the help of pre-heated brass plates and three coins to make a glass sample of uniform thickness. Thereafter, put it in another electric furnace at 350°C for about 2 hours to avoid the thermal strains, air bubbles from the as-prepared glass. Finally, the

Sm^{3+} doped borosilicate glass sample is prepared to study their novel properties. The image of all synthesized glass are shown in Figure 1.

Fig. 1. Image of the synthesized glasses.

The XRD profile of synthesized host glass was observed by a X-ray Bruker D8 Advance Diffractometer. In this instrument, X-ray is generated by Cu-Kα radiation (λ=1.54Å). PL emission and excitation were monitored by Jasco FP-8300 spectrofluorometer. The photoluminescence decay spectral information was recorded by using an Edinburgh FL920 Fluorescence Lifetime Spectrometer. The FT-IR spectrum was monitored via Spectrum Two FT-IR Spectrometer- PerkinElmer.

3. Results and Discussion

3.1. XRD analysis:

Figure 2 depicts the XRD spectrum of the as-synthesized host glass sample. It was monitored in the 2Θ range from 10 to 70 degrees. It clearly differentiates the crystalline and amorphous nature of glass. No distinguishable intense peaks were observed in Fig.2, but a wide-ranging hump has been observed at low scattering angles, which specifies the glassy nature of prepared borosilicate glasses.

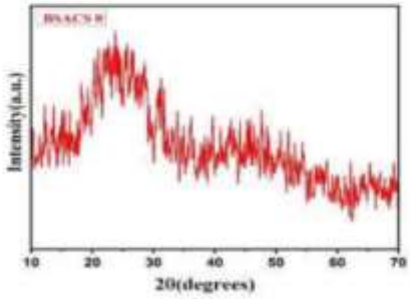

Fig. 2. XRD profile of un-doped borosilicate glass.

3.2. Photoluminescence excitation and emission spectral studies:

It is important to classify the excitation wavelength to explore luminous nature of Samarium ions doped borosilicate glasses. That's why, excitation spectrum was recorded from 300 to 500 nm under a fixed emission wavelength at 599nm. Fig. 3 shows the information pertaining to the excitation spectrum recorded for (0.5mol%) Samarium ions doped as-prepared glass; it confirms the presence of many excitation peaks in the orange region. The details of excitation bands observed at different wavelengths corresponding to the transitions are shown in the Table 1 [6],[13]–[15].

Table 1. The excitation peaks and their corresponding wavelength.

The transition from $^6H_{5/2}\rightarrow$	The excitation bands are centered at the wavelength (λ)
$^4H_{9/2}$	343
$^4D_{3/2}$	360
$^6P_{7/2}$	374
$^4F_{7/2}$	402
$^6M_{19/2}$	416
$^4G_{9/2}$	437
$^4I_{11/2}$	473

After analyzing the excitation spectrum, we found that amongst all peaks, the transition $^6H_{5/2}\rightarrow {}^4F_{7/2}$ (402 nm) shows maximum intensity. The blue spectrum ranging from 500 to 750 nm in Figure 3, depicts the emission profile of as prepared glass (0.5 mol %) near-UV excitation.

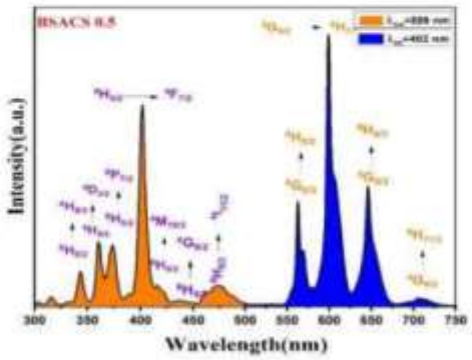

Fig. 3. PL excitation and emission profile of 0.5 mol% Sm^{3+} doped as prepared borosilicate glass.

The emission spectrum contains four peaks centered at different wavelengths corresponding to the transitions are given in Table 2.

Table 2. The emission peaks are centered at wavelength corresponding to transitions

The transition from $^4G_{5/2}\rightarrow$	The excitation bands are centered at the wavelength (λ)
$^6H_{5/2}$	562
$^6H_{7/2}$	599
$^6H_{9/2}$	646
$^6H_{11/2}$	702

After analyzing the emission spectrum, we found that amongst all four peaks, the transition $^4G_{5/2} \rightarrow {}^6H_{7/2}$ (599 nm) shows the maximum intense peak and found in the reddish-orange region.

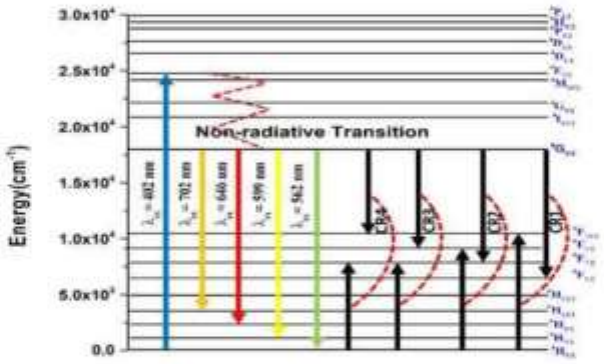

Fig. 4. Energy level diagram of the synthesized glass

Figure 4 depicts energy levels of Samarium ions doped borosilicate glasses. The solid lines denote the radiative transitions and the dashed lines are representing the non-radiative transitions. Due to the minimal energy difference, all excitation thresholds above $^4G_{5/2}$ undergo non-radiative relaxation to this state. The radiative (visible) transitions which are taking place from $^4G_{5/2}$ to different energy states of ^6H_j (j=5/2, 7/2, 9/2 & 11/2) are because there is enough energy gap between them. Because of the small energy gap between closest energy levels, non-radiative transitions occur [6].

3.3. FT-IR spectral analysis:

A pellet of thickness 1 mm is prepared by compressing the mixture of KBr and glass powder in a hydraulic press under high pressure. This pellet is used in a spectrometer to obtain the FT-IR spectra. FT-IR profile of host glass is shown in Figure 5. we get the information of the molecular or rotational vibrations associated with the bonds from

FT-IR spectra. The obtained bands are located at 702, 944, 1045, 1088, 1146, 1298, 1339, 1394, and 1498 cm^{-1} respectively. This figure also contains two broad bands ranging from 2700-3000 cm^{-1} and 3600-3750 cm^{-1}. The band positions and their assigned modes of vibrations present in the glass are presented in Table 3.

Table 3. FT-IR band assignments for the glass sample BSAC: xSm^{3+} (x = 0 mol%)

Peak Positions Wavenumbers (cm^{-1})	Assignments	References
3600–3750	OH Water	[16]
2700–3000	Hydrogen bonding	[17], [18]
~1498	Three nonbridging oxygen atoms of the B-O-B groups produce anti-symmetric stretching vibrations.	[19]
~1394	$B-O$ asymmetric vibration in BO_3^{3-} and BO_2O^- units	[20], [21]
~1339	$B-O$ stretching vibration of pyroborate, meta, and orthoborate groups	[17], [19]
~1298	Symmetric stretching vibration of $B-O$ in BO_3^{-}	[19], [22]
~1146	$B-O$ stretching vibrations of trigonal BO_3^{-} units only	[20]
~1088	Asymmetric stretching vibration of $Si-O-Si$ bonds	[23], [24]
~1045	$B-O$ Stretching vibrations of tetrahedral BO_4^{-} unit	[17]
~944	Stretching vibrations of Si-OH	[25]
~702	$B-O-B$ vibrations in the borate networks	[26], [27]

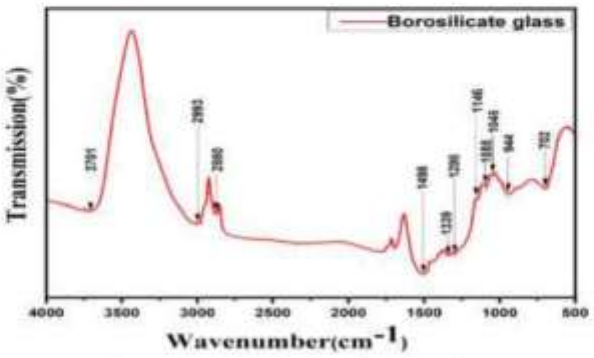

Fig. 5. FT-IR profile of undoped borosilicate glass.

3.4. Photoluminescence lifetime decay curve analysis:

PL decay profiles were monitored at 599nm emission wavelength under 402nm excitation wavelength. The measured results are depicted in Figure 6. The PL decay profiles were plotted in a semi-logarithmic plot and normalized on the maximum intensity. The PL decay curve recorded for BSAC: xSm3+(0.1) was fitted using bi-exponential function:[28]

$$I(t) = A_1 exp\left(-\frac{t}{\tau_1}\right) + A_2 exp(-\frac{t}{\tau_2}) \quad (1)$$

and PL decay curve recorded for BSAC: xSm3+ (0.5 & 1.5) were fitted by using the tri-exponential function:

$$I(t) = A_1 exp\left(-\frac{t}{\tau_1}\right) + A_2 exp\left(-\frac{t}{\tau_2}\right) + A_3 exp(-\frac{t}{\tau_3}) \quad (2)$$

In which constants have their usual meanings. The average decay lifetime τ can be determined by:

$$\tau = \frac{A_1(\tau_1)^2 + A_2(\tau_2)^2 + A_3(\tau_3)^2}{A_1\tau_1 + A_2\tau_2 + A_3\tau_3} \quad (3)$$

The photoluminescence decay profile of Sm^{3+} doped borosilicate glass is depicted in Figure 6, In which glass with concentration 0.1 mol% is fitted bi-exponentially and the other two are fitted tri-exponentially [29]. The average decay time (τ_{avg}) of BSAC: xSm^{3+} (x=0.1, 0.5 and 1.5 mol %) is 2.85 µs, 1.86 µs and 1.36 µs respectively. τ_{avg} of the glasses decrease quickly after increasing the dopant ion concentrations and this happens because of the transfer of energy between Samarium ions at smaller distances.

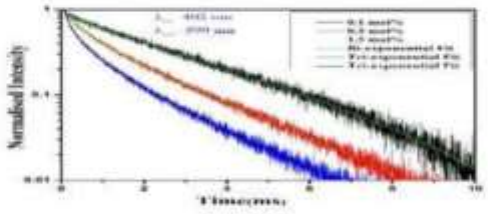

Fig. 6. Photoluminescence decay profile of BSAC:xSm^{3+}(x = 0.1, 0.5, 1.5) samples under 402 nm excitation, monitoring emission at 599 nm.

CIE chromaticity coordinates

The colour emitted from rare-earth ion-doped material can be understood through photoluminescence spectra by using CIE (Commission Internationale de L'Eclairage) chromaticity coordinate system[6], [30]. We need these 4-9 following equations to calculate

chromaticity coordinates. The Planckian radiator is referred to the black body radiation. The spectral power distribution can be calculated by Planck's radiation formula:

$$P(\lambda,T) = 2hc^2\lambda^{-5}\left(\exp\left(\frac{hc}{\lambda k_B T}\right)-1\right)^{-1} \quad (4)$$

Where variables have their usual meanings which are mentioned in Ref[31]. CIE tristimulus is calculated by the following three equations:

$$X(T) = k\int P(\lambda,T)\,\bar{x}(\lambda)d\lambda \quad (5)$$

$$Y(T) = k\int P(\lambda,T)\,\bar{y}(\lambda)d\lambda \quad (6)$$

$$Z(T) = k\int P(\lambda,T)\,\bar{z}(\lambda)d\lambda \quad (7)$$

Where $\bar{x}$, $\bar{y}$ & $\bar{z}$ are CIE colour matching functions (CMFs). And $X(T)$, $Y(T)$, & $Z(T)$ are tristimulus values of CIE 1931 [32], [33] The CIE 1931 chromaticity coordinate is calculated by these two formulae:

$$x = \frac{X(T)}{X(T)+Y(T)+Z(T)} \quad (8)$$

$$y = \frac{Y(T)}{X(T)+Y(T)+Z(T)} \quad (9)$$

We calculated CIE chromaticity coordinates of the Sm+3 doped glass from emission spectra by using the above-given formulae, as shown in Table 4. The CIE 1931 coordinate system assigns a colour to a point on the chromaticity diagram by using two colour coordinates, x, and y. CIE plot with chromaticity coordinates is shown in Figure 7. In this figure, clearly we can see that, coordinates are positioned in reddish-orange region in CIE plot. This shows that this material can be used in reddish-orange luminescent device applications.

Table 4. The color coordinates of CIE diagram.

Glass sample doping concentration Mol %	Colour Coordinates	
	X	y
0.1	0.5842	0.3958
0.5	0.5998	0.3964
1.0	0.5934	0.4005
1.5	0.5871	0.3979
2.0	0.5930	0.4019

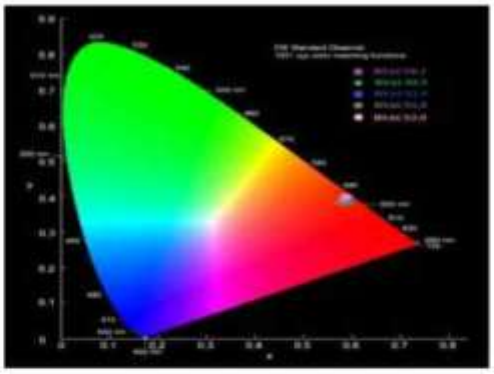

Fig. 7. CIE diagram of Sm^{+3} doped borosilicate glasses.

4. Conclusions

Borosilicate (BSAC: xSm^{3+}) glasses doped with Samarium ions were developed by using melt quench method. Borosilicate glasses are characterized by using XRD, FT-IR, photoluminescence excitation, emission, and PL decay spectral studies to comprehend the use of these materials in photonic device applications. The XRD and FT-IR studies of the host glass sample tells about the amorphous nature and presence of different bonds and functional groups. The most intense peak ($^4G_{5/2} \rightarrow {}^6H_{7/2}$) is centered at 599nm in the PL profile. The experimental lifetime decreases as doping ions concentration increases and this happenes because of the non-radiating transition that takes place between borosilicate glass and Sm^{3+} ions. The coordinates of CIE obtained for an optimum concentration of doping ion in borosilicate (BSAC: xSm^{3+}) glasses are 0.561, 0.435, where x=0.5 mol %. All of the above findings indicate that Sm^{3+} doped borosilicate glass is suitable for its usage in visible reddish orange photonic devices.

References

1. N. Deopa and A. S. Rao, "Spectroscopic studies of Sm3+ ions activated lithium lead alumino borate glasses for visible luminescent device applications," *Optical Materials*, vol. 72, pp. 31–39, 2017, doi: 10.1016/j.optmat.2017.04.067.
2. S. Mahamuda, K. Swapna, M. Venkateswarlu, A. Srinivasa Rao, S. Shakya, and G. Vijaya Prakash, "Spectral characterisation of Sm3+ ions doped Oxy-fluoroborate glasses for visible orange luminescent applications," *Journal of Luminescence*, vol. 154, pp. 410–424, 2014, doi: 10.1016/j.jlumin.2014.05.017.
3. N. Deopa, S. Kaur, A. Prasad, B. Joshi, and A. S. Rao, "Spectral studies of Eu3+ doped lithium lead alumino borate glasses for visible photonic applications," *Optics and Laser Technology*, vol. 108, pp. 434–440, 2018, doi: 10.1016/j.optlastec.2018.07.010.

4. Q. Chen, Q. Chen, and M. Ferraris, "Effect of Ceramic Crucibles on Magneto-Optical PbO-Bi₂O₃-B₂O₃Glasses Properties," *New Journal of Glass and Ceramics*, vol. 02, no. 01, pp. 41–50, 2012, doi: 10.4236/njgc.2012.21007.
5. A. Ghosh and B. K. Chaudhuri, "Preparation and characterization of binary V2O5-Bi2O3 glasses," *Journal of Materials Science*, vol. 22, no. 7, pp. 2369–2376, 1987, doi: 10.1007/BF01082118.
6. N. Deopa, B. Kumar, M. K. Sahu, P. R. Rani, and A. S. Rao, "Effect of Sm 3+ ions concentration on borosilicate glasses for reddish orange luminescent device applications," *Journal of Non-Crystalline Solids*, vol. 513, no. January, pp. 152–158, 2019, doi: 10.1016/j.jnoncrysol.2019.03.025.
7. R. S. Quimby, P. A. Tick, N. F. Borrelli, and L. K. Cornelius, "Quantum efficiency of Pr3+ doped transparent glass ceramics," *Journal of Applied Physics*, vol. 83, no. 3, pp. 1649–1653, 1998, doi: 10.1063/1.366879.
8. R. Van Deun, K. Binnemans, C. Görller-Walrand, and J. L. Adam, "Judd-Ofelt intensity parameters of trivalent lanthanide ions in a NaPO3-BaF2 based fluorophosphate glass," *Journal of Alloys and Compounds*, vol. 283, no. 1–2, pp. 59–66, 1999, doi: 10.1016/S0925-8388(98)00895-0.
9. G. Ravi, C. Madhukar Reddy, L. Manoj, and B. Deva Prasad Raju, "Structural and optical studies of Sm3+ ions doped niobium borotellurite glasses," *Journal of Molecular Structure*, vol. 1029, pp. 53–59, 2012, doi: 10.1016/j.molstruc.2012.06.059.
10. V. Venkatramu, P. Babu, C. K. Jayasankar, T. Tröster, W. Sievers, and G. Wortmann, "Optical spectroscopy of Sm3+ ions in phosphate and fluorophosphate glasses," *Optical Materials*, vol. 29, no. 11, pp. 1429–1439, 2007, doi: 10.1016/j.optmat.2006.06.011.
11. K. Swapna, S. Mahamuda, A. S. Rao, T. Sasikala, and L. R. Moorthy, "Visible luminescence characteristics of Sm3+ doped Zinc Alumino Bismuth Borate glasses," *Journal of Luminescence*, vol. 146, pp. 288–294, 2014, doi: 10.1016/j.jlumin.2013.09.035.
12. K. K. Mahato, D. K. Rai, and S. B. Rai, "Optical studies of Sm3+ doped oxyfluoroborate glass," *Solid State Communications*, vol. 108, no. 9, pp. 671–676, 1998, doi: 10.1016/S0038-1098(98)00442-6.
13. Q. Xu, D. Xu, and J. Sun, "Preparation and luminescence properties of orange-red Ba3Y(PO4)3:Sm3+ phosphors," *Optical Materials*, vol. 42, pp. 210–214, 2015, doi: 10.1016/j.optmat.2014.12.035.
14. D. Tu, Y. Liang, R. Liu, Z. Cheng, F. Yang, and W. Yang, "Photoluminescent properties of LiSrxBa1-xPO 4:RE3+ (RE = Sm3+, Eu3+) f-f transition phosphors," *Journal of Alloys and Compounds*, vol. 509, no. 18, pp. 5596–5599, 2011, doi: 10.1016/j.jallcom.2011.02.077.
15. G. Seeta Rama Raju, J. S. Yu, J. Y. Park, H. C. Jung, and B. K. Moon, "Photoluminescence and cathodoluminescence properties of nanocrystalline Ca 2Gd 8Si 6O 26: Sm 3+ phosphors," *Journal of the American Ceramic Society*, vol. 95, no. 1, pp. 238–242, 2012, doi: 10.1111/j.1551-2916.2011.04762.x.
16. T. A. Taha and A. S. Abouhaswa, "Preparation and optical properties of borate glass doped with MnO2," *Journal of Materials Science: Materials in Electronics*, vol. 29, no. 10, pp. 8100–8106, 2018, doi: 10.1007/s10854-018-8816-7.
17. C. Gautam, A. K. Yadav, and A. K. Singh, "A Review on Infrared Spectroscopy of Borate Glasses with Effects of Different Additives," *ISRN Ceramics*, vol. 2012, pp. 1–17, 2012, doi: 10.5402/2012/428497.
18. K. Marimuthu, R. T. Karunakaran, S. Surendra Babu, G. Muralidharan, S. Arumugam, and C. K. Jayasankar, "Structural and spectroscopic investigations on Eu3+-doped alkali

fluoroborate glasses," *Solid State Sciences*, vol. 11, no. 7, pp. 1297–1302, 2009, doi: 10.1016/j.solidstatesciences.2009.04.011.
19. P. P. Pawar, S. R. Munishwar, and R. S. Gedam, "Physical and optical properties of Dy3+/Pr3+ Co-doped lithium borate glasses for W-LED," *Journal of Alloys and Compounds*, vol. 660, pp. 347–355, 2016, doi: 10.1016/j.jallcom.2015.11.087.
20. M. R. Ahmed and M. Shareefuddin, "EPR, optical, physical and structural studies of strontium alumino-borate glasses containing Cu2+ ions," *SN Applied Sciences*, vol. 1, no. 3, 2019, doi: 10.1007/s42452-019-0201-5.
21. T. A. Taha and A. S. Abouhaswa, "Preparation and optical properties of borate glass doped with MnO2," *Journal of Materials Science: Materials in Electronics*, vol. 29, no. 10, pp. 8100–8106, 2018, doi: 10.1007/s10854-018-8816-7.
22. I. Ardelean, S. Cora, and D. Rusu, "EPR and FT-IR spectroscopic studies of Bi2O3- B 2O3-CuO glasses," *Physica B: Condensed Matter*, vol. 403, no. 19–20, pp. 3682–3685, 2008, doi: 10.1016/j.physb.2008.06.016.
23. T. Xiu, Q. Liu, and J. Wang, "Alkali-free borosilicate glasses with wormhole-like mesopores," *Journal of Materials Chemistry*, vol. 16, no. 41, pp. 4022–4024, 2006, doi: 10.1039/b612215a.
24. G. Shao *et al.*, "Thermal shock behavior and infrared radiation property of integrative insulations consisting of MoSi2/borosilicate glass coating and fibrous ZrO2 ceramic substrate," *Surface and Coatings Technology*, vol. 270, no. May 2015, pp. 154–163, 2015, doi: 10.1016/j.surfcoat.2015.03.008.
25. S. T. Wang, M. L. Chen, and Y. Q. Feng, "A meso-macroporous borosilicate monolith prepared by a sol-gel method," *Microporous and Mesoporous Materials*, vol. 151, pp. 250–254, 2012, doi: 10.1016/j.micromeso.2011.10.029.
26. M. Diantoro, N. D. Prastiwi, A. Taufiq, N. Hidayat, N. Mufti, and A. Hidayat, "The Role of Fe2O3 and Light Induced on Dielectric Properties of Borosilicate Glass," *Journal of Physics: Conference Series*, vol. 846, no. 1, pp. 1–6, 2017, doi: 10.1088/1742-6596/846/1/012007.
27. A. A. Aleni, H. Sedghi, A. R. Mirmohseni, and V. Golsanamlu, "Synthesis and characterization of cadmium doped lead-borate glasses," *Bulletin of Materials Science*, vol. 29, no. 1, pp. 55–58, 2006, doi: 10.1007/BF02709356.
28. D. Wang, P. Zhang, Q. Ma, J. Zhang, and Y. Wang, "Synthesis, optical properties and application of Y 7 O 6 F 9 :Er 3+ for sensing the chip temperature of a light emitting diode," *Journal of Materials Chemistry C*, vol. 6, no. 48, pp. 13352–13358, 2018, doi: 10.1039/c8tc05307c.
29. G. Swati *et al.*, "Investigation on luminescence enhancement and decay characteristics of long afterglow nanophosphors for dark-vision display applications," *Applied Surface Science*, vol. 333, pp. 178–185, 2015, doi: 10.1016/j.apsusc.2015.01.135.
30. C. S. McCamy, "Correlated color temperature as an explicit function of chromaticity coordinates," *Color Research & Application*, vol. 17, no. 2, pp. 142–144, 1992, doi: 10.1002/col.5080170211.
31. R. C. Dougal, "The presentation of the Planck radiation formula (tutorial)," *Physics Education*, vol. 11, no. 6, pp. 438–443, 1976, doi: 10.1088/0031-9120/11/6/008.
32. D. B. Judd, "The 1931 I C I Standard Observer and Coordinate System for Colorimetrya,b," *Journal of the Optical Society of America*, vol. 23, no. 10, p. 359, 1933, doi: 10.1364/josa.23.000359.
33. C. Li *et al.*, "Accurate method for computing correlated color temperature," *Optics Express*, vol. 24, no. 13, p. 14066, 2016, doi: 10.1364/oe.24.014066.